Graphene Nanoribbons and Carbon Nanotubes

Branislav K. Nikolić

Department of Physics and Astronomy, University of Delaware, Newark, DE 19716, U.S.A.

http://wiki.physics.udel.edu/phys824

From Bulk Graphene Lattice to GNRs

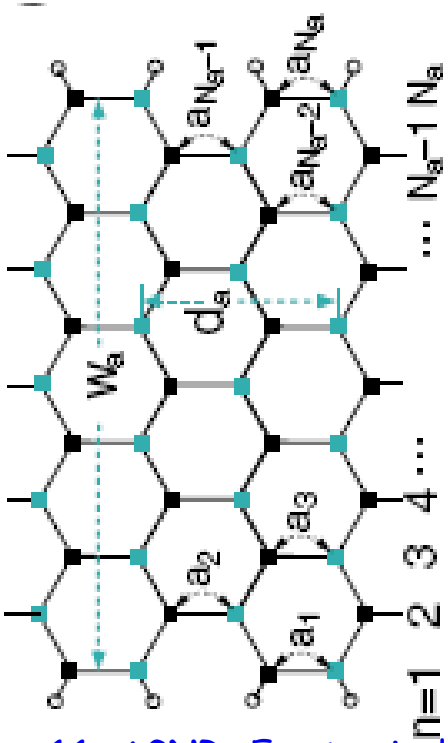

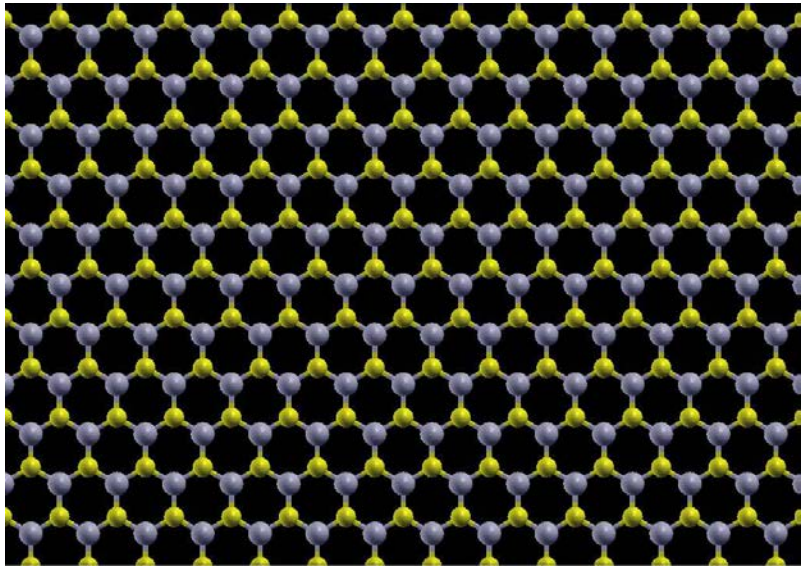

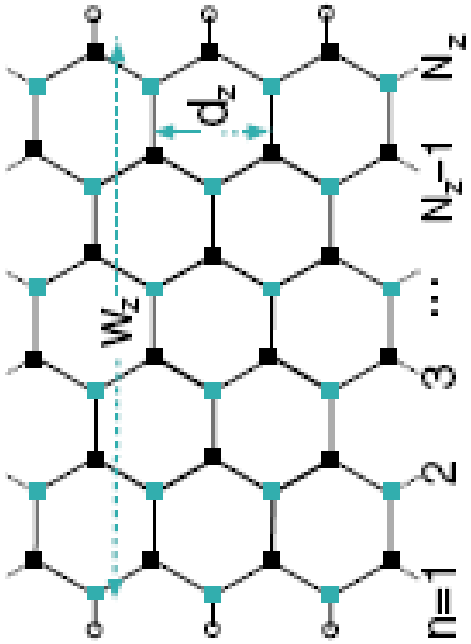

11-AGNR: Empty circles denote hydrogen atoms passivating the edge carbon atoms, and the black and gray rectangles represent atomic sites belonging to different sublattices of the honeycomb lattice of graphene. The 1D unit cell (or supercell) distance and ribbon width are represented by d_a and W_a, respectively. The carbon-carbon distance on the n-th dimer line is denoted as a_n.

6-ZGNR: The empty circles and rectangles follow the same convetion as for AGNR. The 1D unit cell (or supercell) distance and the ribbon width are denoted as d_z and W_z, respectively.

From Bulk Graphene Lattice to Single-Wall CNTs

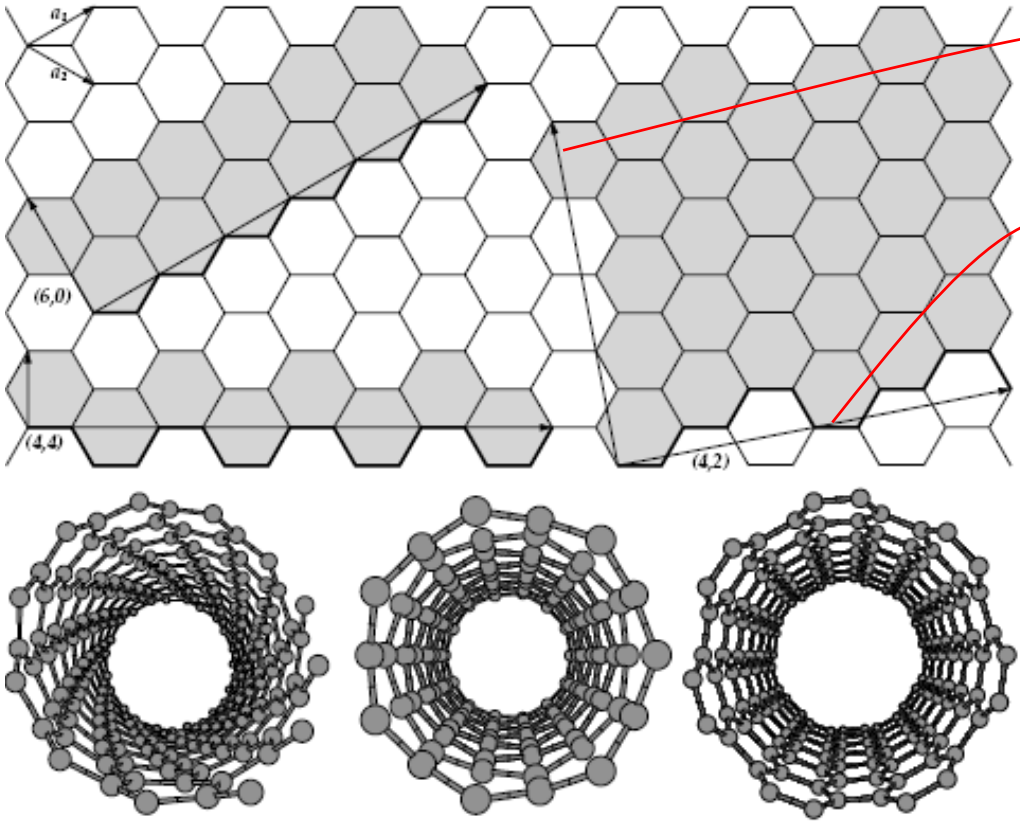

Figure 13.9. **Top:** a graphene sheet with the ideal lattice vectors denoted as $\mathbf{a}_1, \mathbf{a}_2$. The thicker lines show the edge profile of a (6, 0) (zig-zag), a (4, 4) (armchair), and a (4, 2) (chiral) tube. The tubes are formed by matching the end-points of these profiles. The hexagons that form the basic repeat unit of each tube are shaded, and the thicker arrows indicate the repeat vectors along the axis of the tube and perpendicular to it, when the tube is unfolded. **Bottom:** perspective views of the (8, 4) chiral tube, the (7, 0) zig-zag tube and the (7, 7) armchair tube along their axes.

$$a_{\perp}^{(n,m)} = n\mathbf{a}_1 + m\mathbf{a}_2 = na\left[\frac{(1+\kappa)\sqrt{3}}{2}\hat{\mathbf{x}} + \frac{1-\kappa}{2}\hat{\mathbf{y}}\right]$$

$$a_{\parallel}^{(n,m)} = a\left[\frac{\kappa-1}{2}\hat{\mathbf{x}} + \frac{(1+\kappa)\sqrt{3}}{2}\hat{\mathbf{y}}\right]\frac{\lambda\sqrt{3}}{1+\kappa+\kappa^2}$$

$\kappa = n/m$

λ = smallest rational number that produces $\mathbf{a}_{\parallel}^{(n,m)}$ as the graphene lattice vector

TABLE I. Structural parameters for a (n,m) carbon nanotube. In this table, n, m, t_1, t_2 are integers.

Symbol	Name	Formula	Value
a	lattice constant	$a=\sqrt{3}a_{cc}\simeq 2.46$ Å	$a_{cc}\simeq 1.42$ Å
$\mathbf{a}_1$, $\mathbf{a}_2$	basis vectors	$\left(\frac{\sqrt{3}}{2};\frac{1}{2}\right)a, \left(\frac{\sqrt{3}}{2};-\frac{1}{2}\right)a$	
$\mathbf{b}_1$, $\mathbf{b}_2$	reciprocal-lattice vectors	$\left(\frac{1}{\sqrt{3}};1\right)\frac{2\pi}{a}, \left(\frac{1}{\sqrt{3}};-1\right)\frac{2\pi}{a}$	
$\mathbf{C}_h$	chiral vector	$\mathbf{C}_h=n\mathbf{a}_1+m\mathbf{a}_2\equiv(n,m)$	$(0\leqslant\lvert m\rvert\leqslant n)$
d_t	tube diameter	$d_t=\frac{\lvert\mathbf{C}_h\rvert}{\pi}=\frac{a}{\pi}\sqrt{n^2+nm+m^2}$	
θ	chiral angle	$\sin\theta=\frac{\sqrt{3}m}{2\sqrt{n^2+nm+m^2}}$	$0\leqslant\lvert\theta\rvert\leqslant\frac{\pi}{6}$
		$\cos\theta=\frac{2n+m}{2\sqrt{n^2+nm+m^2}}$	$\tan\theta=\frac{\sqrt{3}m}{2n+m}$
$\mathbf{T}$	translational vector	$\mathbf{T}=t_1\mathbf{a}_1+t_2\mathbf{a}_2\equiv(t_1,t_2)$	$\gcd(t_1,t_2)=1$[a]
		$t_1=\frac{2m+n}{N_R}, t_2=-\frac{2n+m}{N_R}$	$N_R=\gcd(2m+n,2n+m)$[a]
N_C	number of C atoms per unit cell	$N_C=\frac{4(n^2+nm+m^2)}{N_R}$	

[a] $\gcd(n,m)$ denotes the greatest common divisor of the two integers n and m.

Terminology: (n,0) – zigzag CNT | (n,n) – armchair CNT | (n,m) n≠m chiral CNT | m<n gives unique def.

Zigzag and Armchair CNTs are NOT Related to Zigzag and Armchair GNRs

zigzag CNT

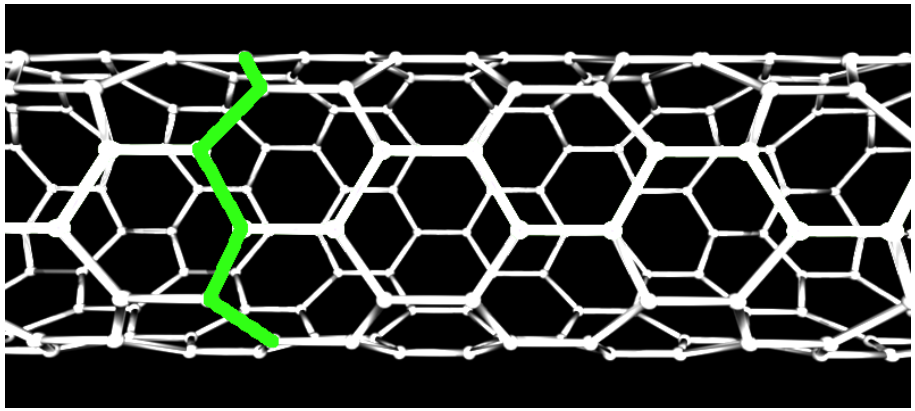

armchair CNT

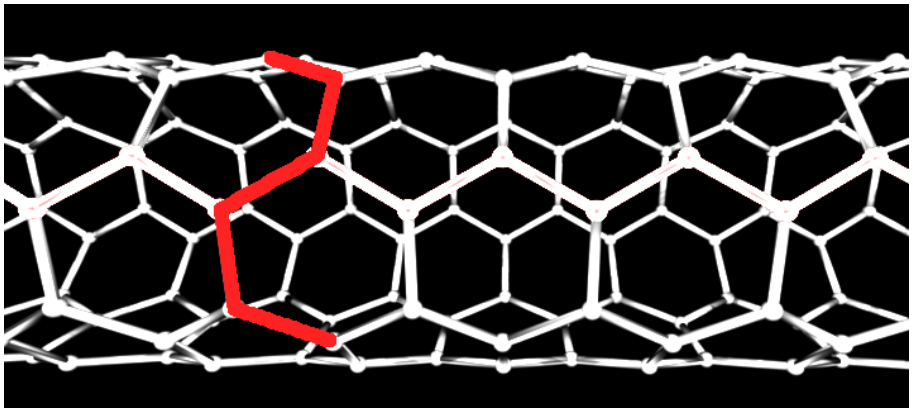

STM image of single-wall CNT

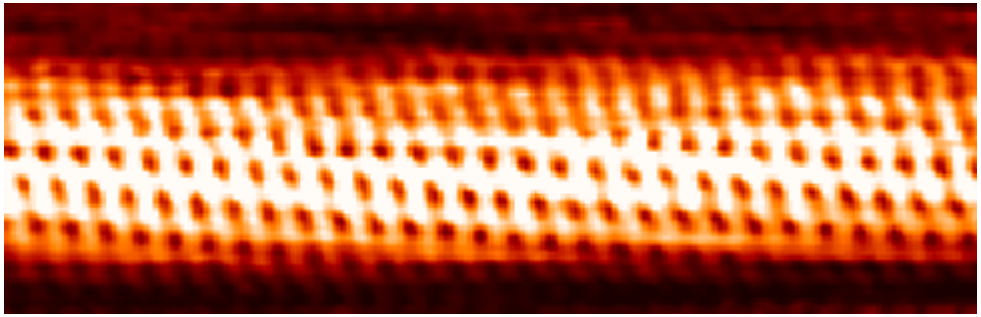

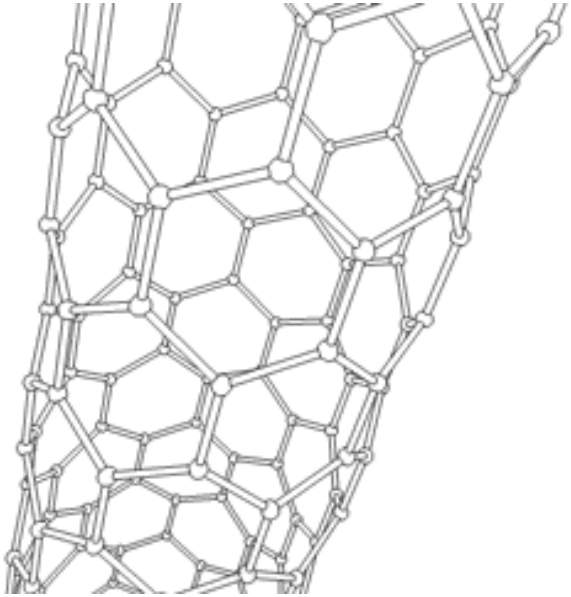

How to Compute Subband Structure of a Quantum Wire Defined on Tight-Binding Lattice

$$\mathbf{H}_{i,i} \equiv \mathbf{H}_0$$

$$\mathbf{H}_{i,i-1} \equiv \mathbf{H}_1$$

The supercell should be sufficiently large so that matrix elements of the Hamiltonian and ovelap matrix have non-zero values only for elements corresponding to the orbitals within the given supercell, or wih its nearest-neighbor cells only.

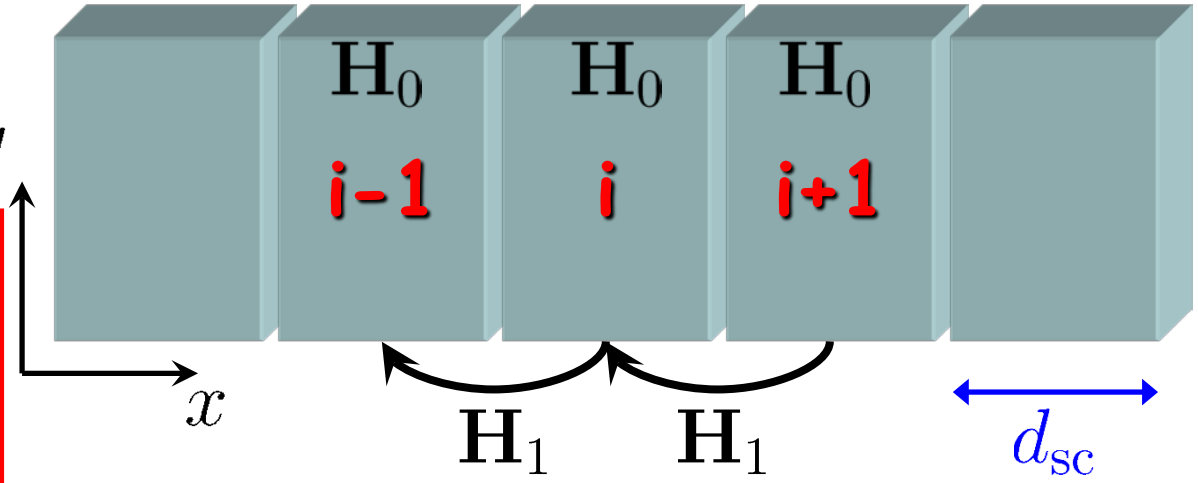

$$\hat{H}\Psi(\mathbf{r}) = E\Psi(\mathbf{r})$$

$$\left[\hat{H}, \hat{P}_x\right] = 0 \Longrightarrow \Psi(x,y) = e^{ik_x d_{\mathrm{sc}} n_x}\chi_{k_x}(y)$$

$$(e^{-ik_x d_{\mathrm{sc}}}\mathbf{H}_1 + \mathbf{H}_0 + e^{ik_x d_{\mathrm{sc}}}\mathbf{H}_1^{\dagger})\chi_{k_x}(y) = E(k_x)\chi_{k_x}(y)$$

Application to GNR: Supercells and Block Matrix Structure of TB Hamiltonian

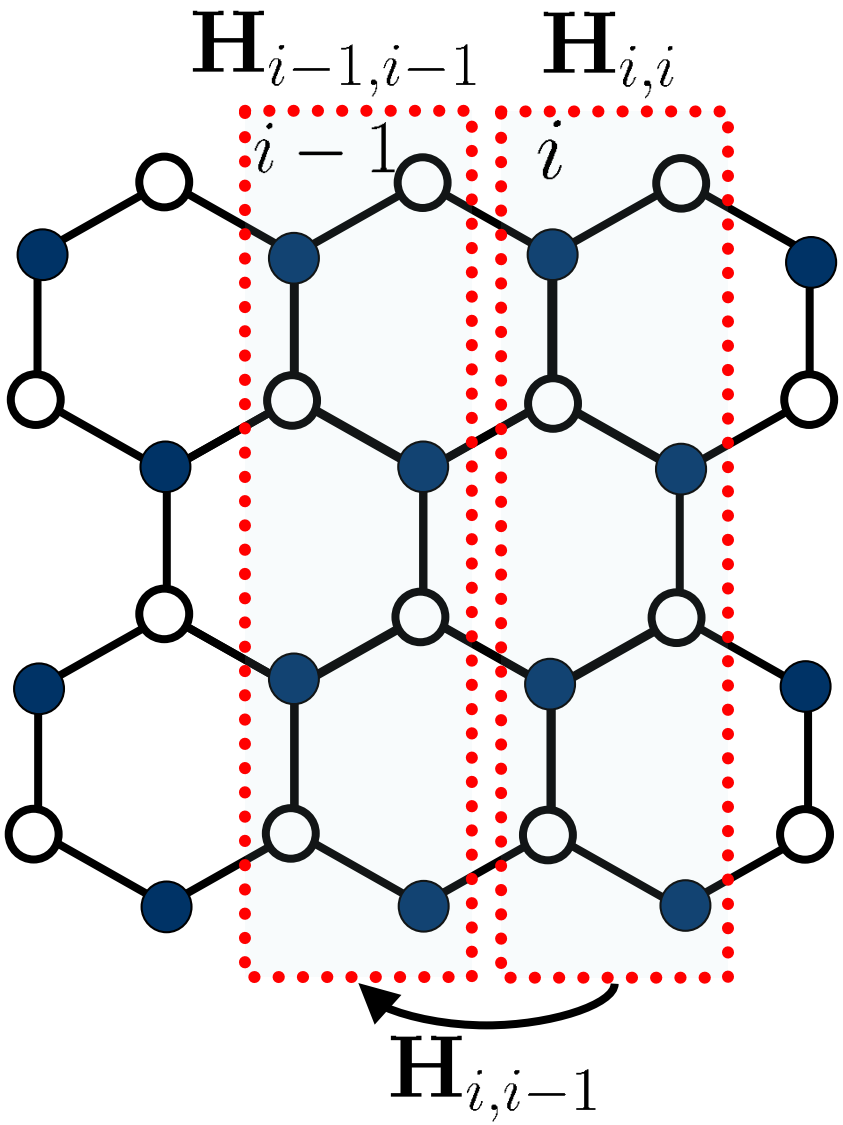

$$\mathbf{H}_{i,i} = -\begin{pmatrix} 0 & t & 0 & 0 & t & 0 & 0 & 0 \\ t & 0 & 0 & 0 & 0 & t & 0 & 0 \\ 0 & 0 & 0 & t & 0 & 0 & t & 0 \\ 0 & 0 & t & 0 & 0 & 0 & 0 & t \\ t & 0 & 0 & 0 & 0 & 0 & 0 & 0 \\ 0 & t & 0 & 0 & 0 & 0 & t & 0 \\ 0 & 0 & t & 0 & 0 & t & 0 & 0 \\ 0 & 0 & 0 & t & 0 & 0 & 0 & 0 \end{pmatrix}$$

$$\mathbf{H}_{i,i-1} = -\begin{pmatrix} 0 & 0 & 0 & 0 & t & 0 & 0 & 0 \\ 0 & 0 & 0 & 0 & 0 & t & 0 & 0 \\ 0 & 0 & 0 & 0 & 0 & 0 & t & 0 \\ 0 & 0 & 0 & 0 & 0 & 0 & 0 & t \\ 0 & 0 & 0 & 0 & 0 & 0 & 0 & 0 \\ 0 & 0 & 0 & 0 & 0 & 0 & 0 & 0 \\ 0 & 0 & 0 & 0 & 0 & 0 & 0 & 0 \\ 0 & 0 & 0 & 0 & 0 & 0 & 0 & 0 \end{pmatrix}$$

GNR in Equilibrium: Subband Structure and the Corresponding Density of States

ARMCHAIR GNR

$N_a = 4$

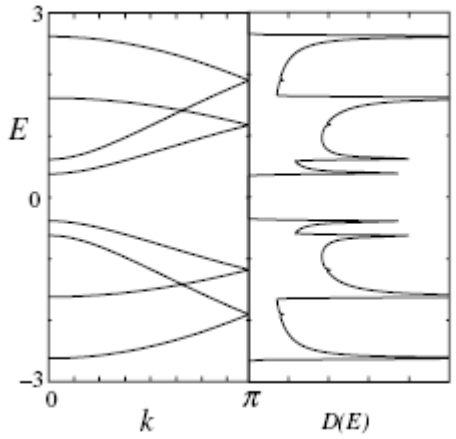

$N_a = 5$

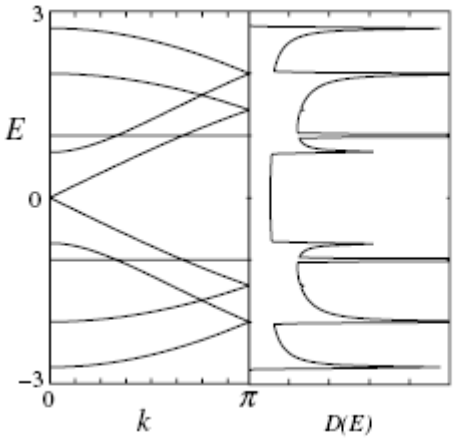

$N_a = 30$

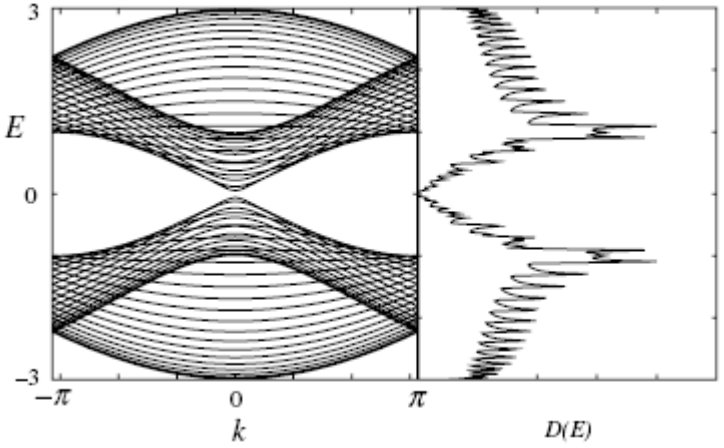

ZIGZAG GNR

$N_z = 4$

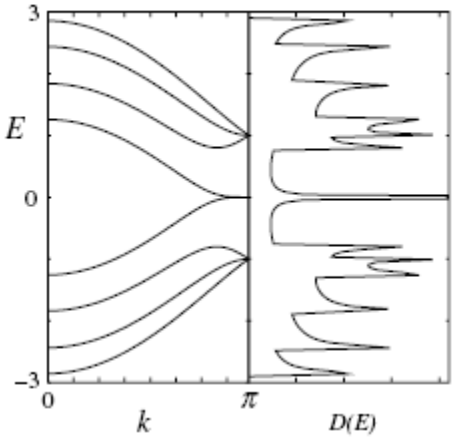

$N_z = 5$

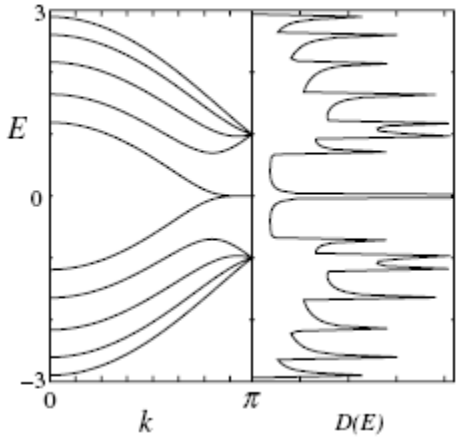

$N_z = 30$

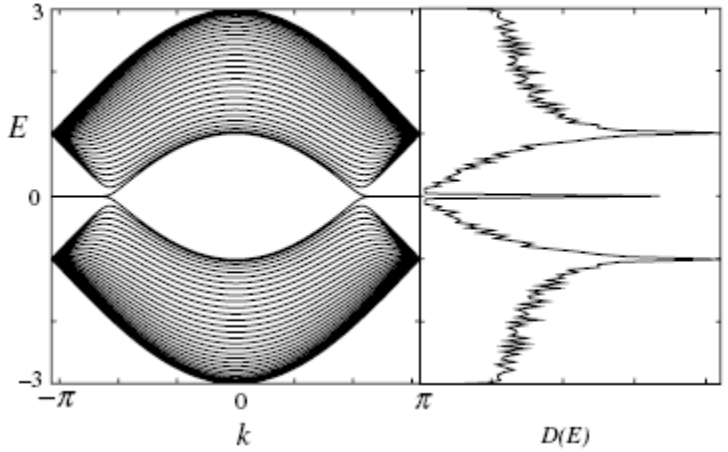

Experimental Methods to Fabricate GNRs

Science **319**, 1229 (2008): Chemical Derivation

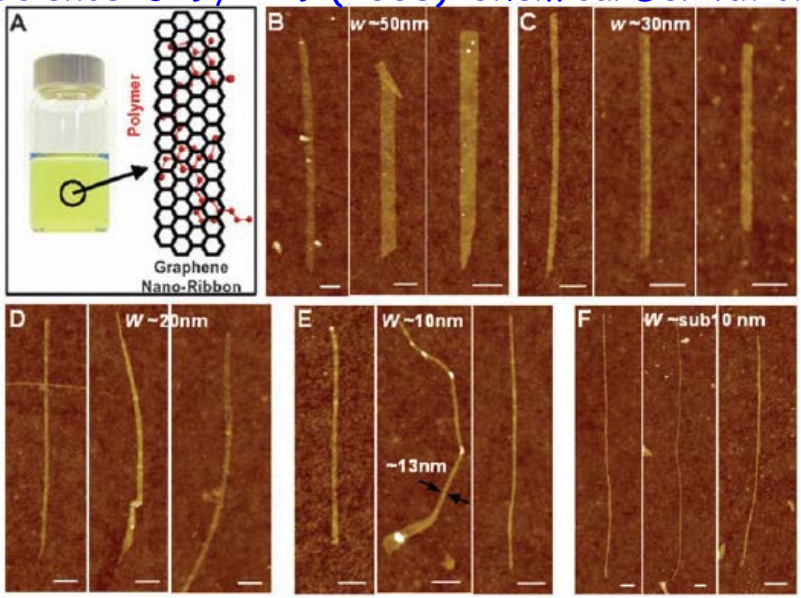

Nature **458**, 872 (2009): SWCNT Unzipping

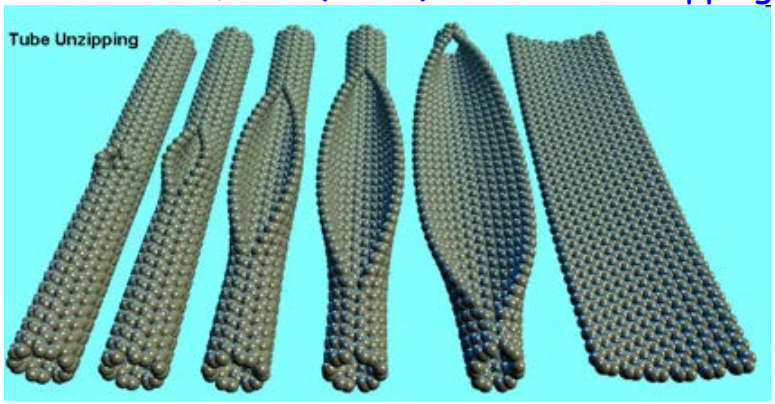

Nature Nanotech. **3**, 397 (2008): STM Nanolithography

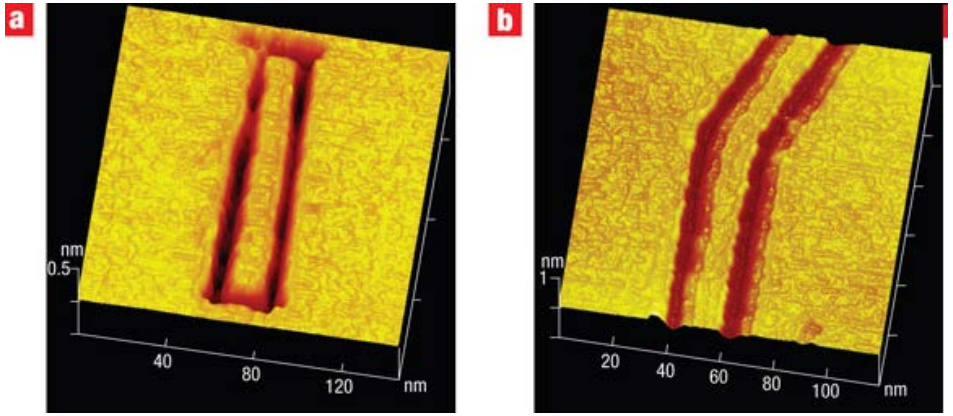

Band vs. Transport Gaps in GNRs with Rough Edges: Coulomb Blockade Effects

PHYSICAL REVIEW B 81, 193408 (2010)

Magnetotransport through graphene nanoribbons

Jeroen B. Oostinga,[1,2] Benjamin Sacépé,[1] Monica F. Craciun,[3] and Alberto F. Morpurgo[1]

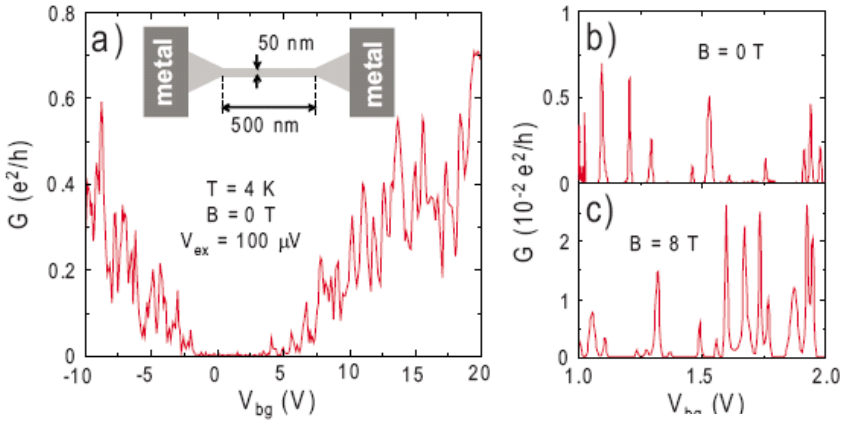

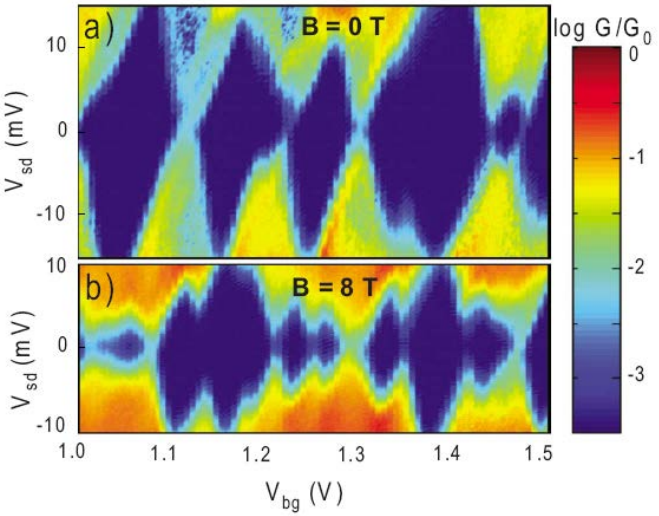

IOP Publishing
Semicond. Sci. Technol. 25 (2010) 034002 (7pp)
Semiconductor Science and Technology
doi:10.1088/0268-1242/25/3/034002

Energy and transport gaps in etched graphene nanoribbons

F Molitor, C Stampfer, J Güttinger, A Jacobsen, T Ihn and K Ensslin

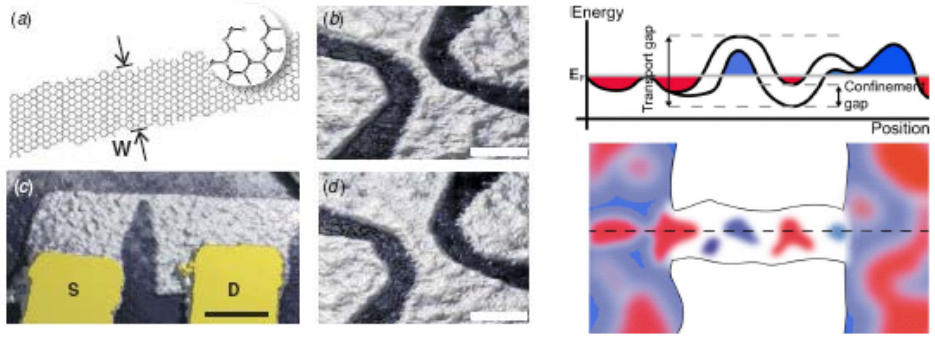

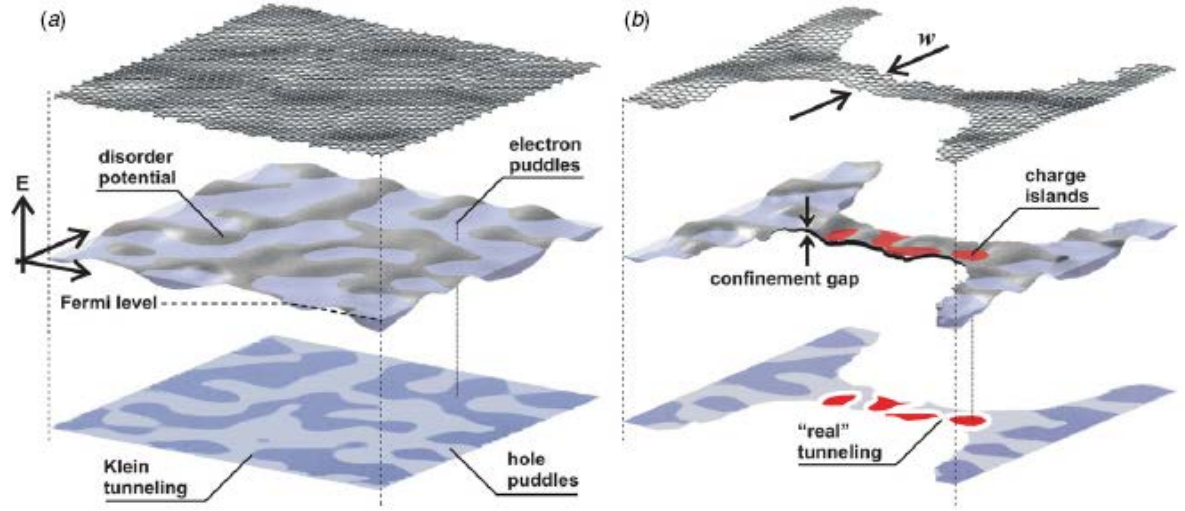

Controlled Formation of GNR Edges: Top-Down vs. Bottom-Up Approaches

top-down

SCIENCE VOL 323 27 MARCH 2009

Controlled Formation of Sharp Zigzag and Armchair Edges in Graphitic Nanoribbons

Xiaoting Jia,[1] Mario Hofmann,[2] Vincent Meunier,[3] Bobby G. Sumpter,[3] Jessica Campos-Delgado,[4] José Manuel Romo-Herrera,[4] Hyungbin Son,[2] Ya-Ping Hsieh,[2] Alfonso Reina,[1] Jing Kong,[2] Mauricio Terrones,[4] Mildred S. Dresselhaus[2,5]*

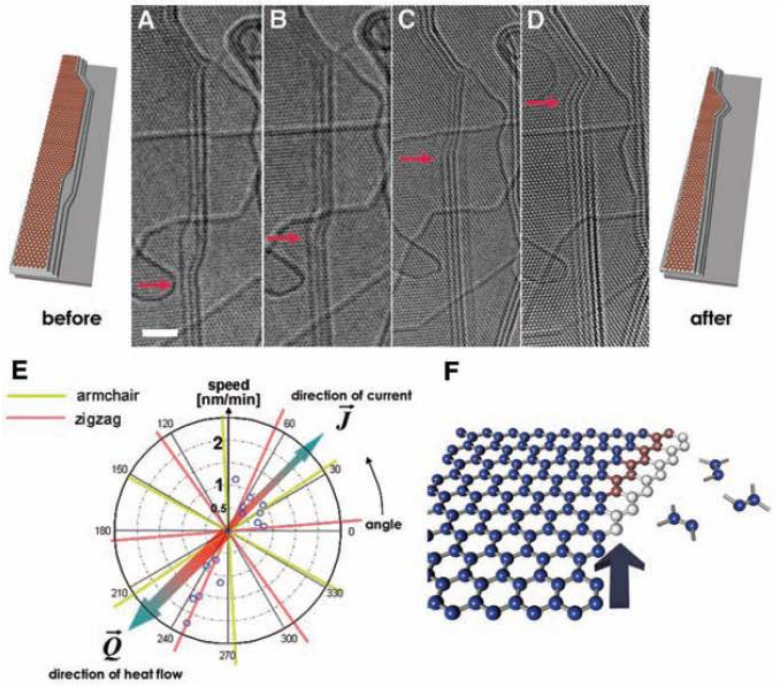

bottom-up

nature Vol 466|22 July 2010|doi:10.1038/nature09211

LETTERS

Atomically precise bottom-up fabrication of graphene nanoribbons

Jinming Cai[1]*, Pascal Ruffieux[1]*, Rached Jaafar[1], Marco Bieri[1], Thomas Braun[1], Stephan Blankenburg[1], Matthias Muoth[2], Ari P. Seitsonen[3,4], Moussa Saleh[5], Xinliang Feng[5], Klaus Müllen[5] & Roman Fasel[1,6]

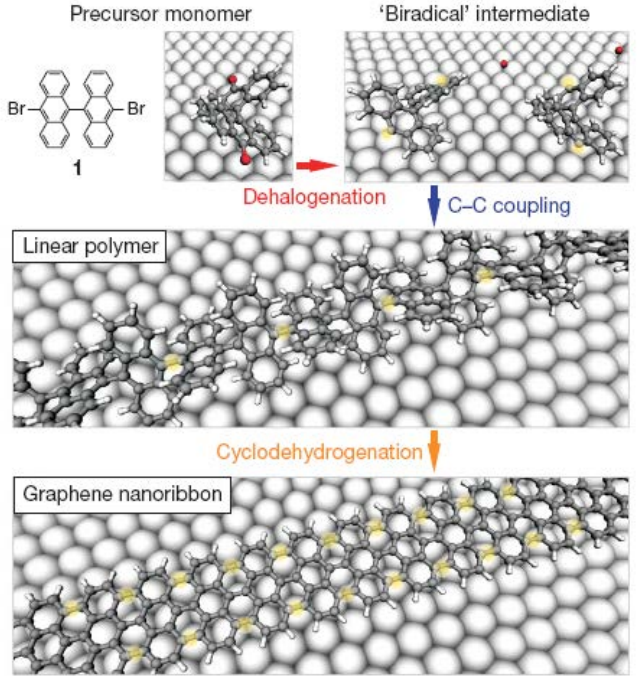

GNRs out of Equilibrium: Conductance Quantization Theory

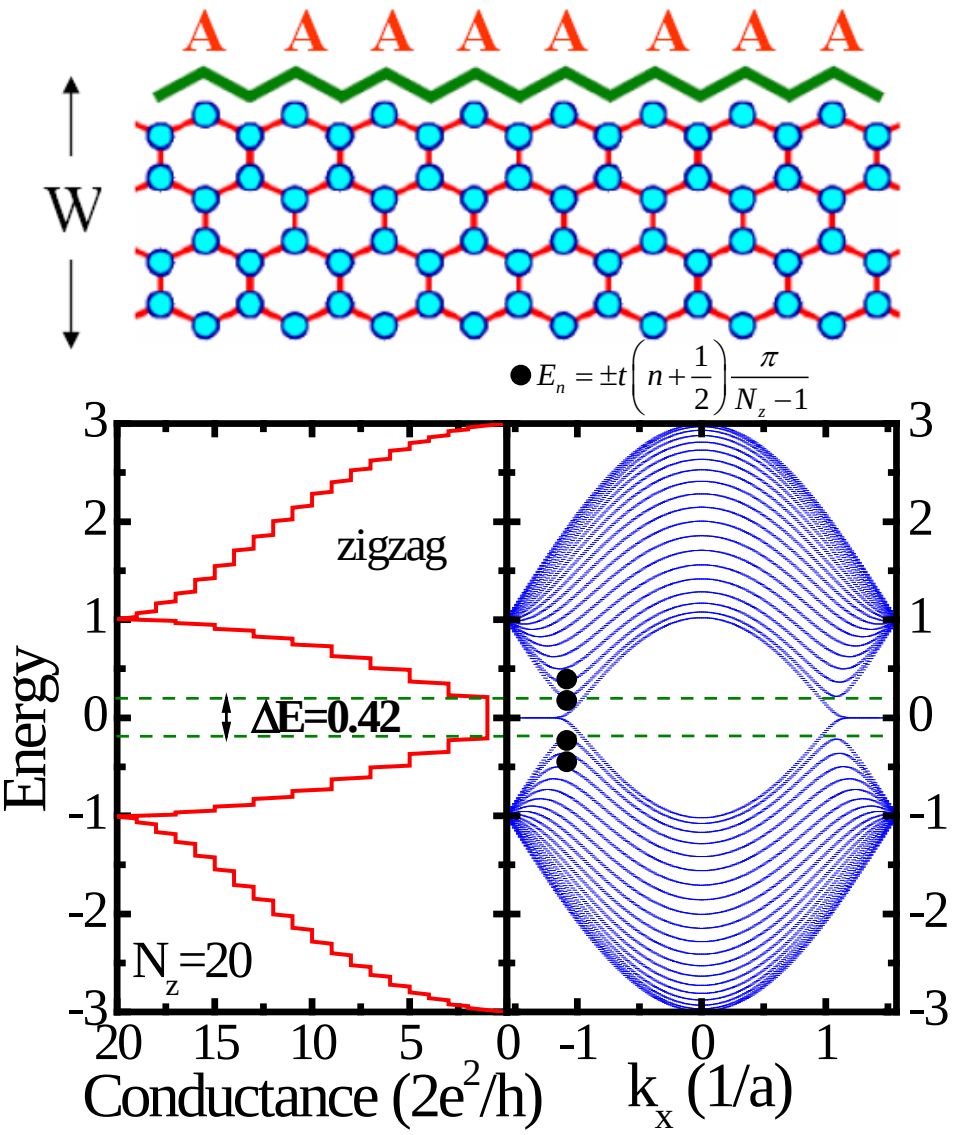

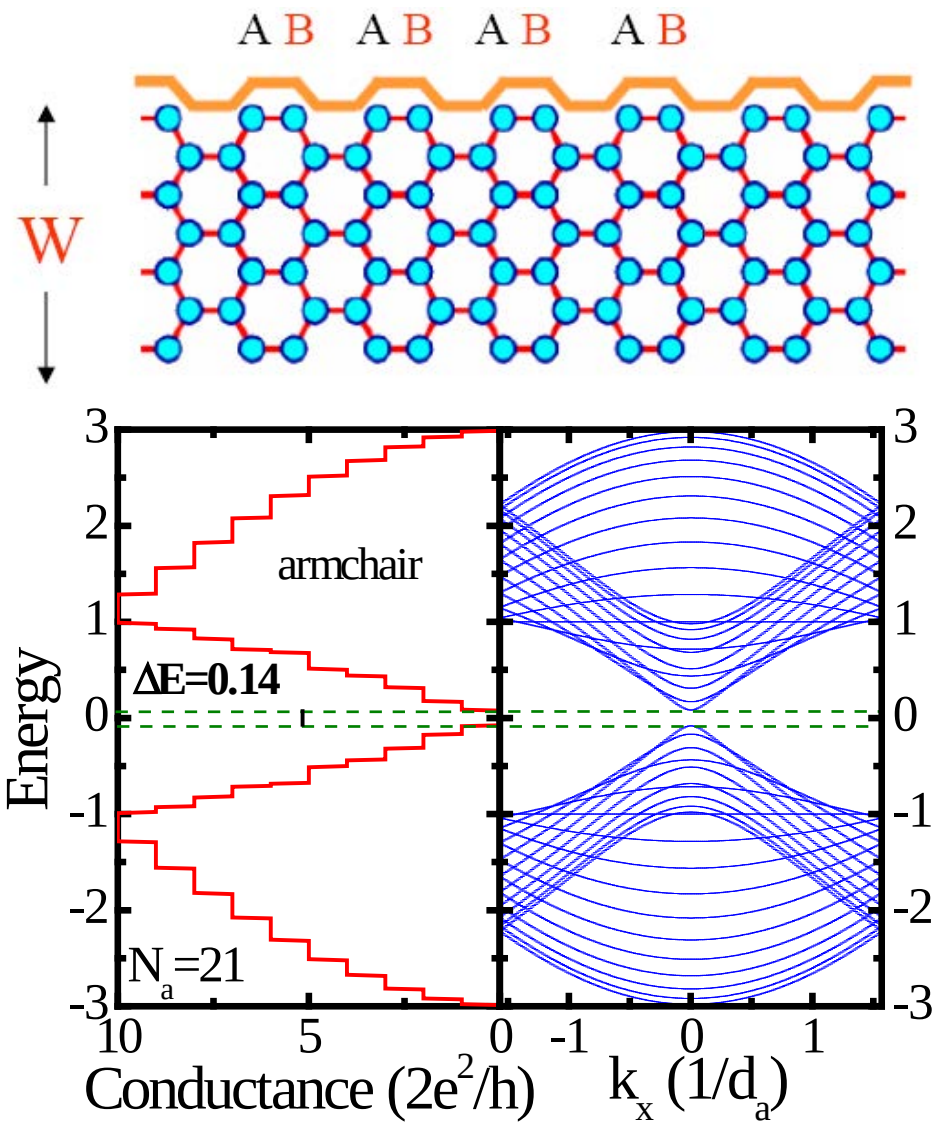

GNR out of Equilibrium: Conductance Quantization Experiment

PRL **60**, 848 (1988)

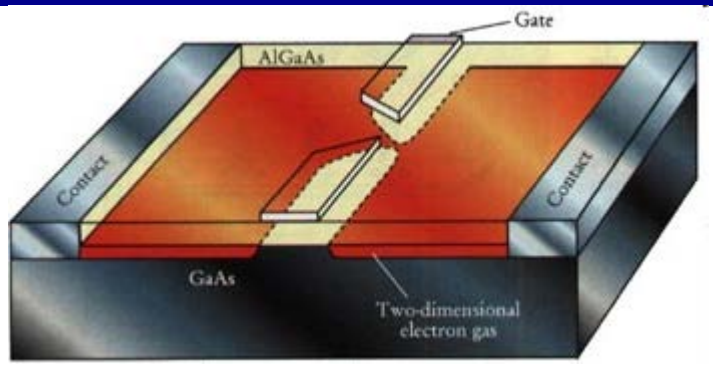

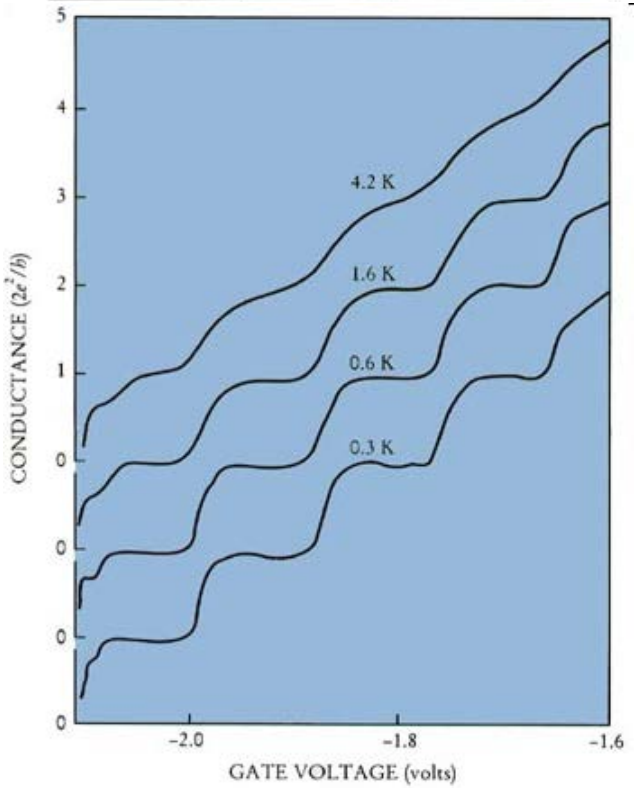

PRB **78**, 161409(R) (2008)

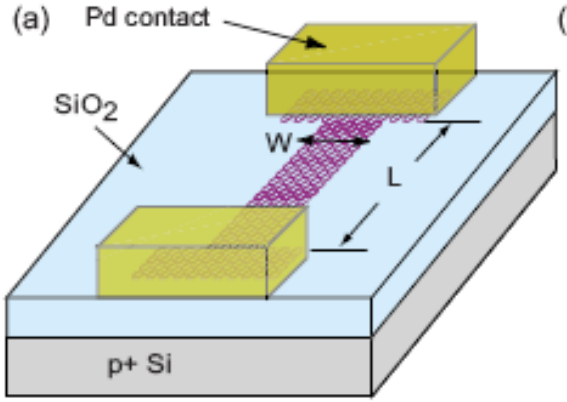

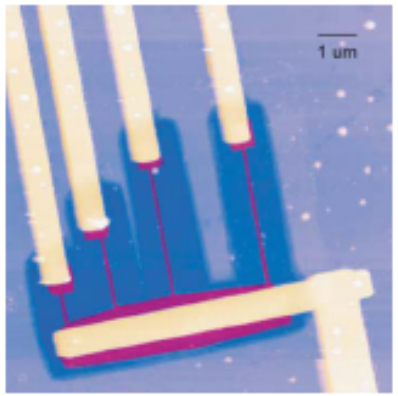

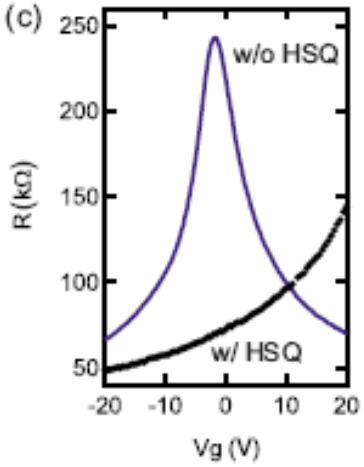

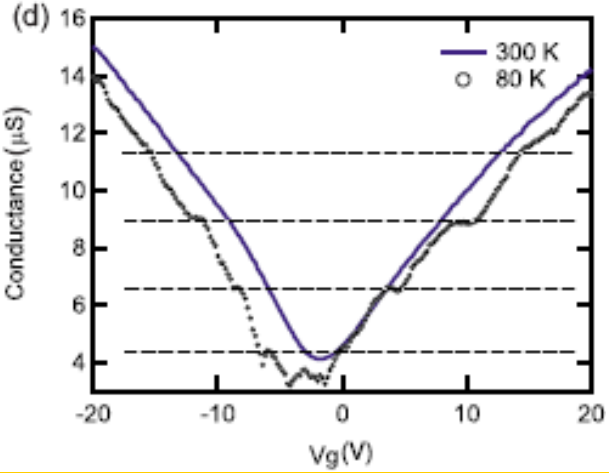

Gated ZGNR: Ballistic Transport Turns Into "Pseudo-Diffusive"

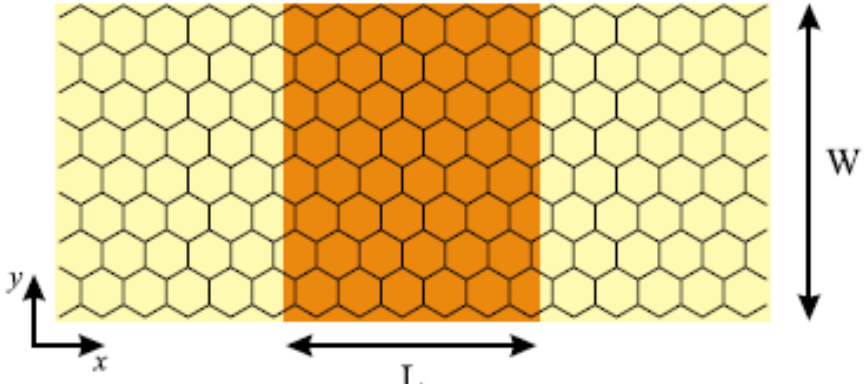

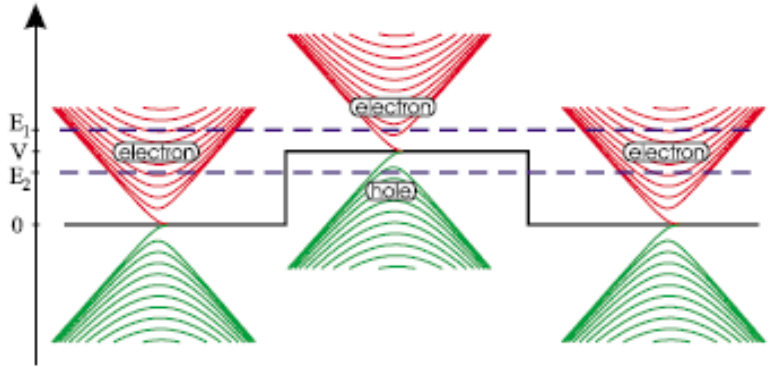

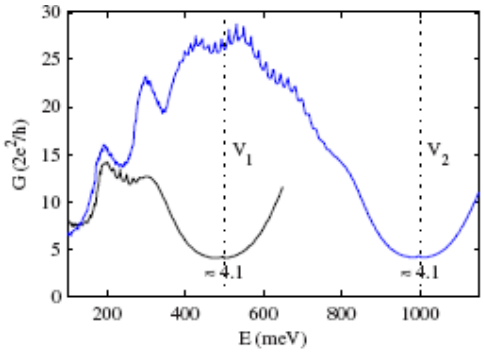

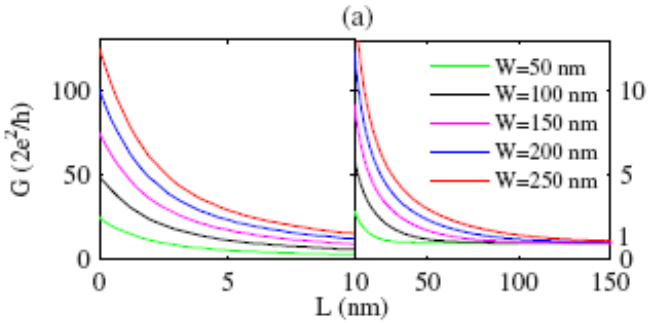

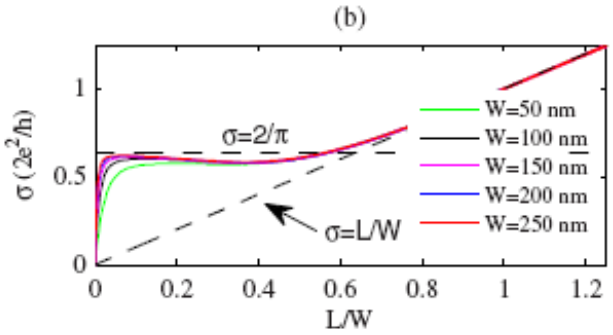

FIG. 5. (Color online) (a) Conductance of graphene ribbons as a function of L. The gate potential is $V=0.5$ eV, the Fermi energy is $E=0.505$ eV, and the ribbon widths are $W=50$, 100, 150, 200, and 250 nm (higher curves of G correspond to increasing values of W). (b) Conductivity $\sigma(E)=G(E)L/W$ for the same samples. The horizontal dotted line corresponds to $\sigma=2/\pi$ (in units $2e^2/h$); the other dotted line corresponds to $\sigma=L/W$ (in units $2e^2/h$). (In the small parameter region $L/W \ll 0.05$, higher curves of σ correspond to increasing values of W).

PRB **76**, 205433 (2007)

Electronic Structure of CNTs: From Graphene via BZ Folding Method

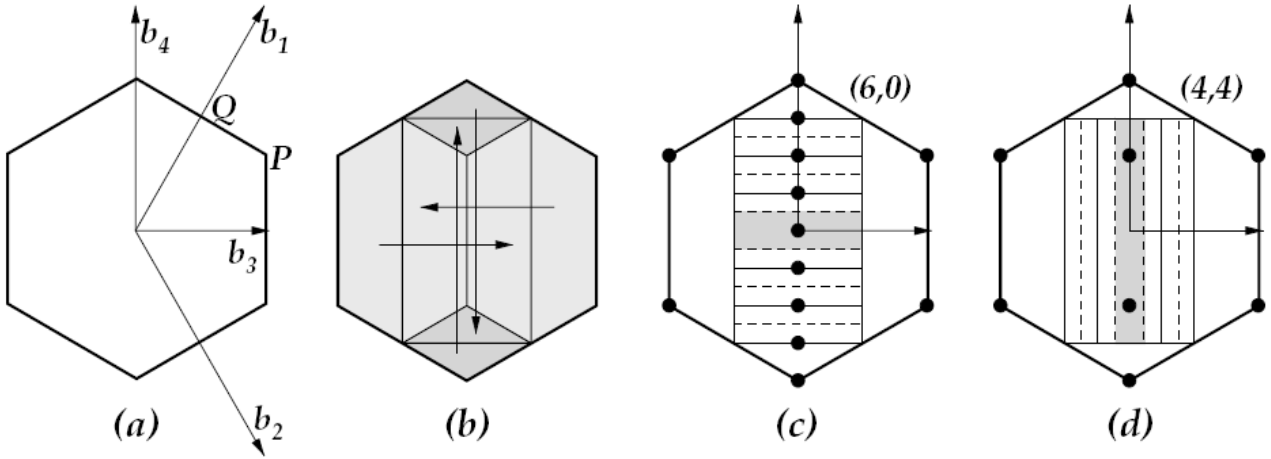

Figure 13.10. (a) The graphene Brillouin Zone, with the reciprocal lattice vectors $\mathbf{b}_1$, $\mathbf{b}_2$ and the tube-related vectors $\mathbf{b}_3$, $\mathbf{b}_4$. (b) The folding of the full zone into the reduced zone, determined by the vectors $\mathbf{b}_3$, $\mathbf{b}_4$. (c) The Brillouin Zone for $(n, 0)$ tubes, and the example of the (6,0) tube: solid lines indicate sets of points equivalent to the $k_y = 0$ line, and dashed lines indicate zone boundaries. (d) The Brillouin Zone for (n, n) tubes, and the example of the (4,4) tube: solid lines indicate sets of points equivalent to the $k_x = 0$ line, and dashed lines indicate zone boundaries. The black dots in (c) and (d) are the images of the point P of the graphene BZ under the folding introduced by the tube structure.

(5,5) ACNT

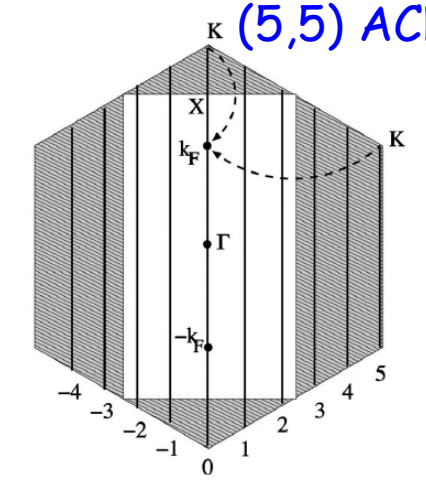

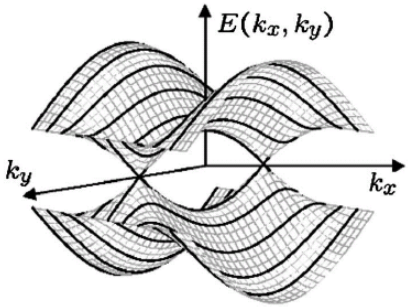

	armchair (n,n)	zigzag (n,0)	chiral (n,m)
metallic	all metalic	n=3p	2n+m=3l
semiconducting		n≠3p	2n+m ≠ 3l

Metallic 1D energy bands are generally unstable under a Peierls distortion → CNT are exception since their tubular structure impedes this effects making their metallic properties at the level of a single molecule rather unique!

CNTs in Equilibrium: Subband Structure and the Corresponding Density of States

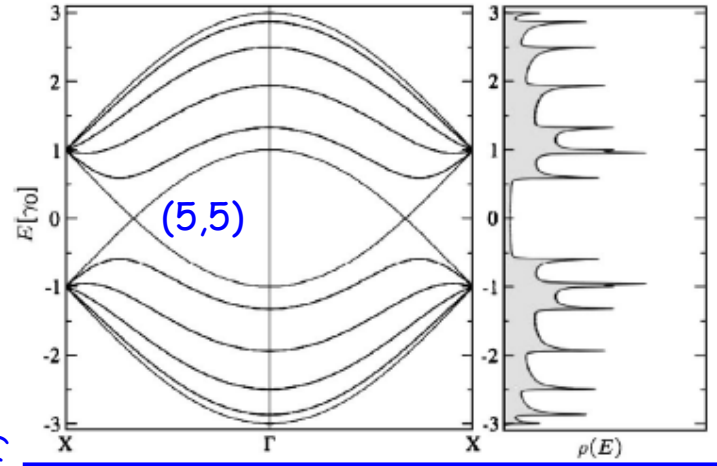

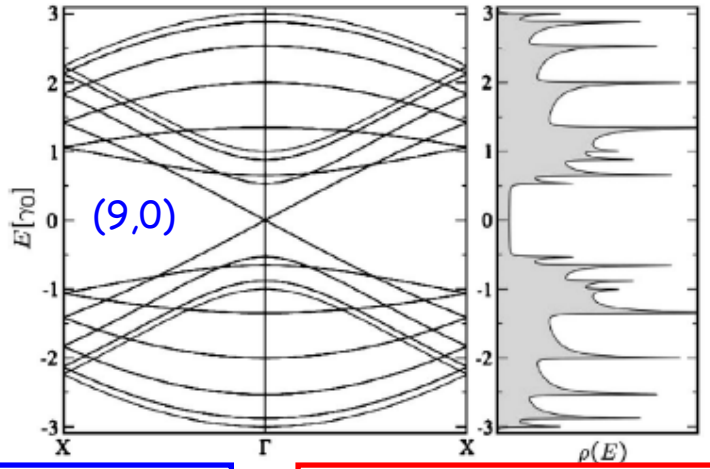

$$\rho(E) = \frac{2}{\Omega}\sum_q \sum_{s=\pm} \int dk\,\delta(E - E_q^s(k)) = \frac{2}{\Omega}\sum_q \sum_{s=\pm} \int dk\,\delta(k - k_{qs}) \left|\frac{\partial E_q^s(k)}{\partial k}\right|^{-1} \left|\frac{\partial E_q^s(k)}{\partial k}\right|^{-1} = \frac{2}{\sqrt{3}\gamma_0 a}\frac{|E_q^s(k)|}{\sqrt{(E_q^s)^2(k) - \varepsilon_{qs}^2}}$$

$$\Rightarrow \quad \rho(E) = \frac{2a}{\pi\gamma_0|\mathbf{C}_h|}\sum_{q=1}^{2n}\sum_{s=\pm}\frac{|E_q^s(k)|}{\sqrt{(E_q^s)^2(k) - \varepsilon_{qs}^2}}$$

RMP **79**, 677 (2007)

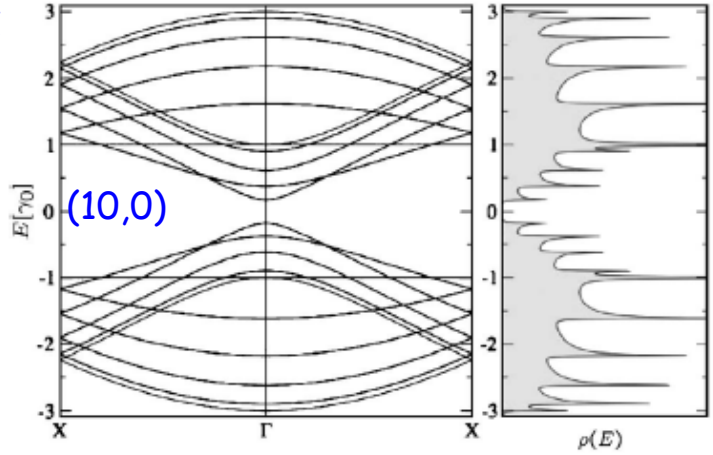

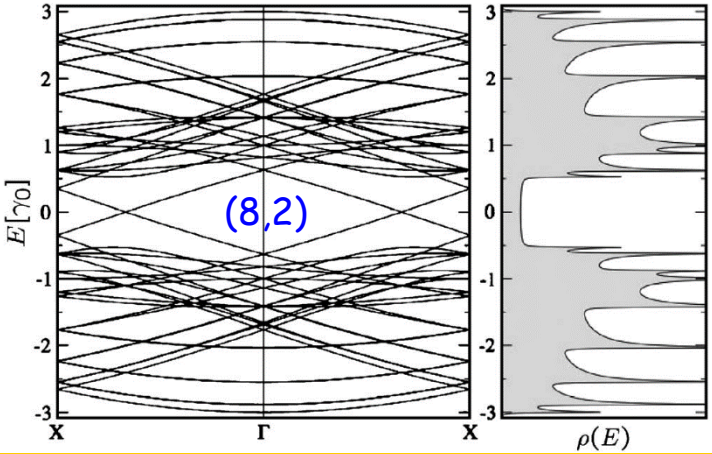

CNTs out of Equilibrium: Conductance Quantization Theory

Infinite metallic (5,5) armchair CNT

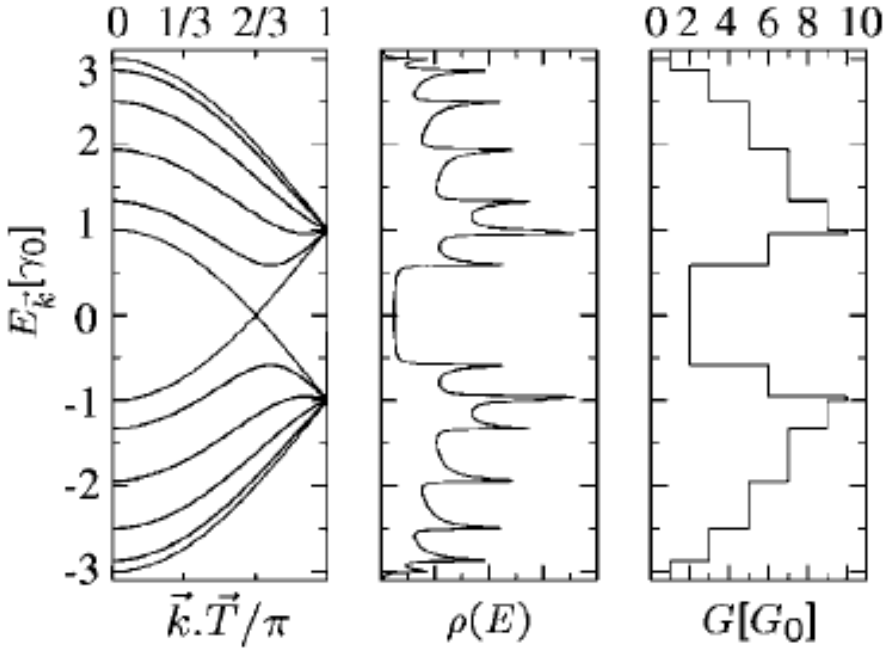

RMP **79**, 677 (2007)

CNT-CNT Junction

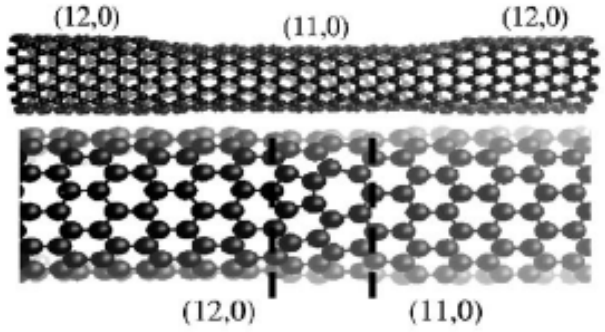

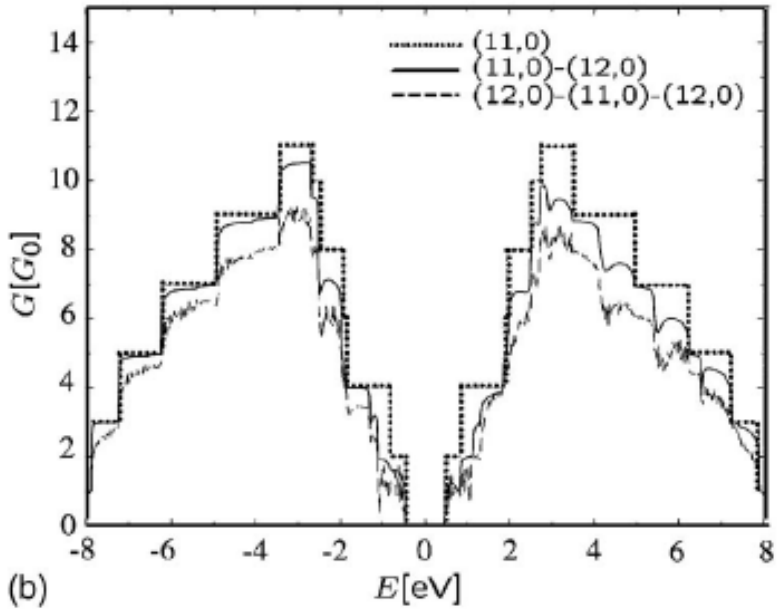

CNTs out of Equilibrium: Conductance Quantization Experiment

Science
AAAS

Carbon Nanotube Quantum Resistors
Stefan Frank, *et al.*
Science **280**, 1744 (1998);
DOI: 10.1126/science.280.5370.1744

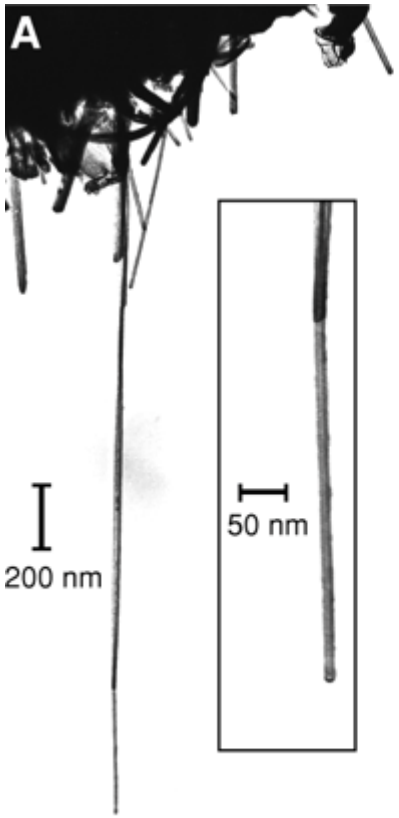

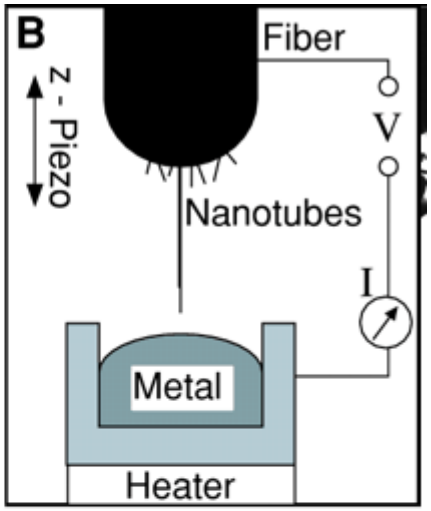

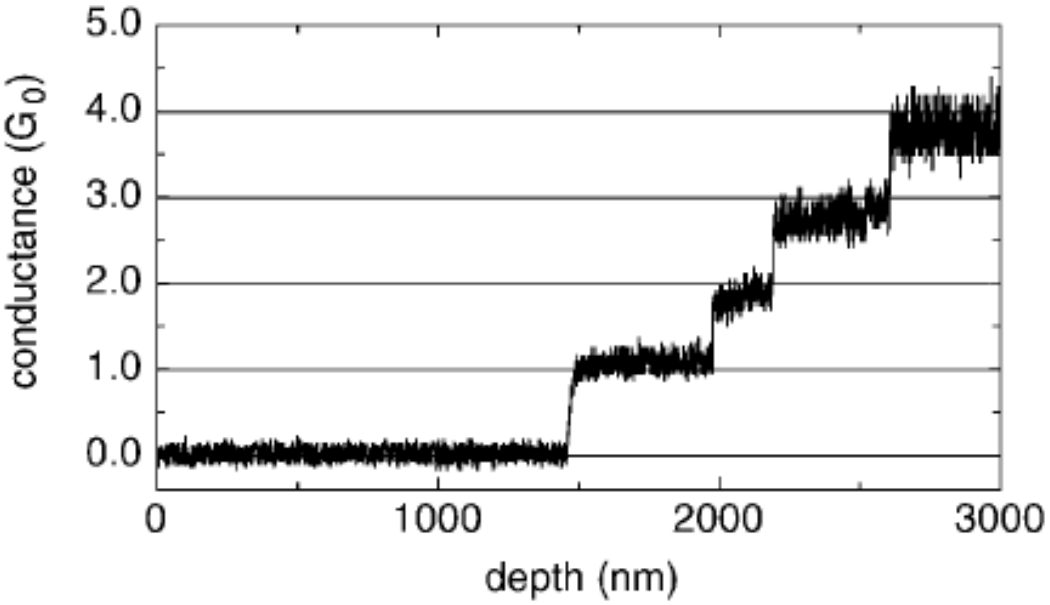

GNR and CNT Subband Structure: Simplistic Tight-Binding Hamiltonians vs. DFT

Nano Res (2008) 1: 361–394
DOI 10.1007/s12274-008-8043-2
Review Article

Charge Transport in Disordered Graphene-Based Low Dimensional Materials

Alessandro Cresti[1,2], Norbert Nemec[3], Blanca Biel[1,2], Gabriel Niebler[4,5], François Triozon[1], Gianaurelio Cuniberti[4], and Stephan Roche[2] (✉)

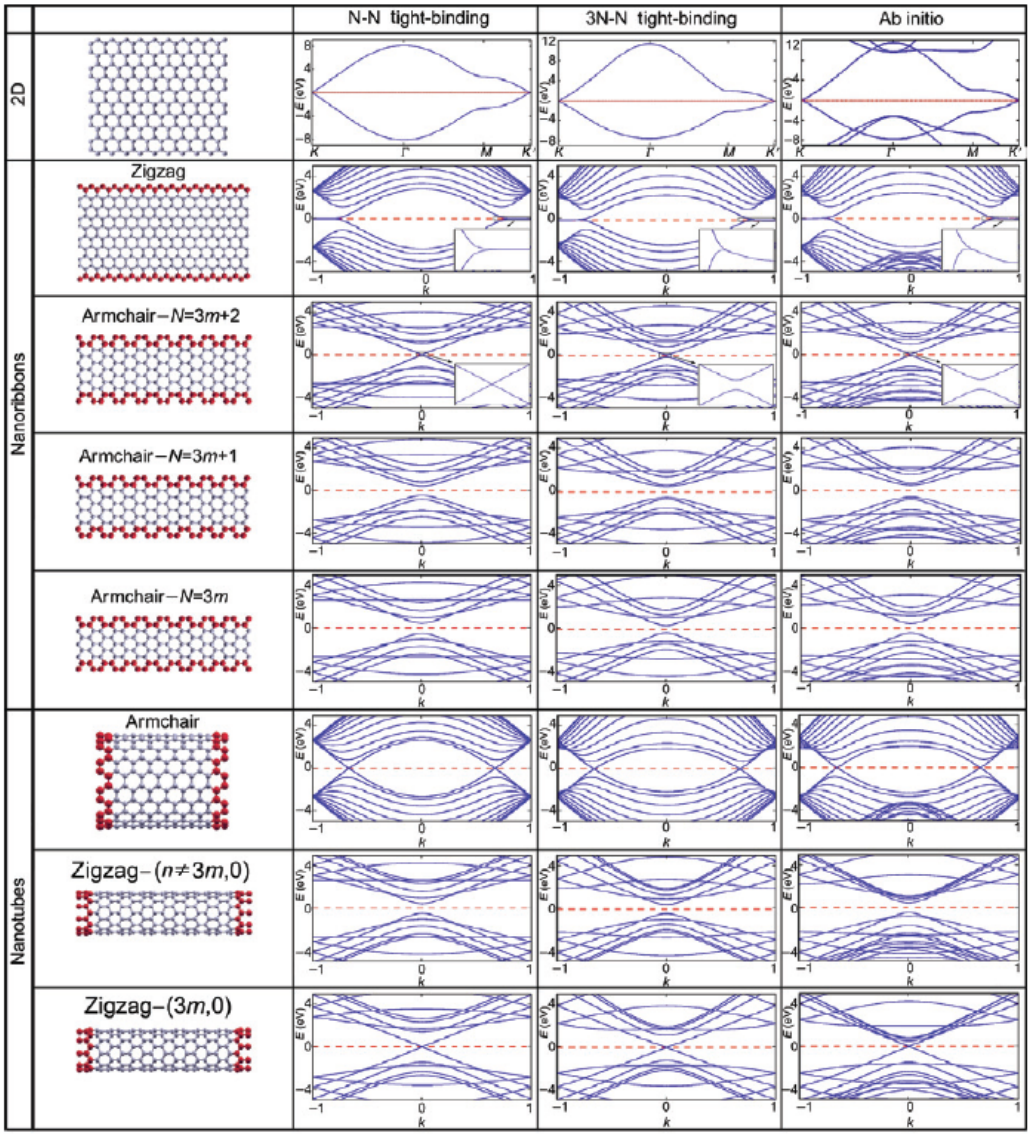

True band structure, as obtained from DFT, is also affected by the curvature of the CNT and variations in the bond lengths which are not all equivalent. The effect are more pronounced in CNT of small diameter, but they do not alter significantly the simple picture based on electronic structure of graphene.

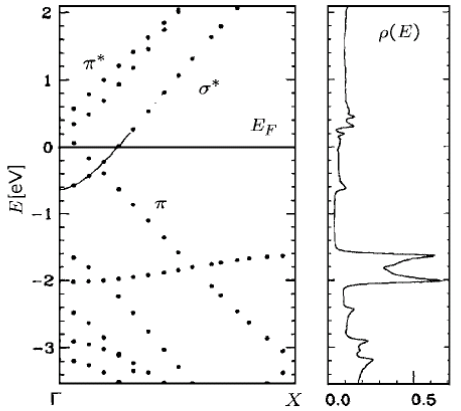

FIG. 21. *Ab initio* electronic band structure and density of states of a (6,0) carbon nanotube, illustrating the strong hybridization that occurs between π and σ states in a small-diameter tube. A new band σ^* appears and crosses the π states around the center of the Brillouin zone. The Fermi level is at zero energy. Adapted from Blase, Benedict, Shirley, and Louie, 1994.

New Channel Materials for Nanoscale FETs: AGNR vs. Semiconducting CNTs

PRL 100, 206803 (2008) PHYSICAL REVIEW LETTERS week ending 23 MAY 2008

Room-Temperature All-Semiconducting Sub-10-nm Graphene Nanoribbon Field-Effect Transistors

Xinran Wang,[1] Yijian Ouyang,[2] Xiaolin Li,[1] Hailiang Wang,[1] Jing Guo,[2] and Hongjie Dai[1,*]

[1]*Department of Chemistry and Laboratory for Advanced Materials, Stanford University, Stanford, California 94305, USA*

[2]*Department of Electrical and Computer Engineering, University of Florida, Gainesville, Florida 32611, USA*

(Received 21 March 2008; published 20 May 2008)

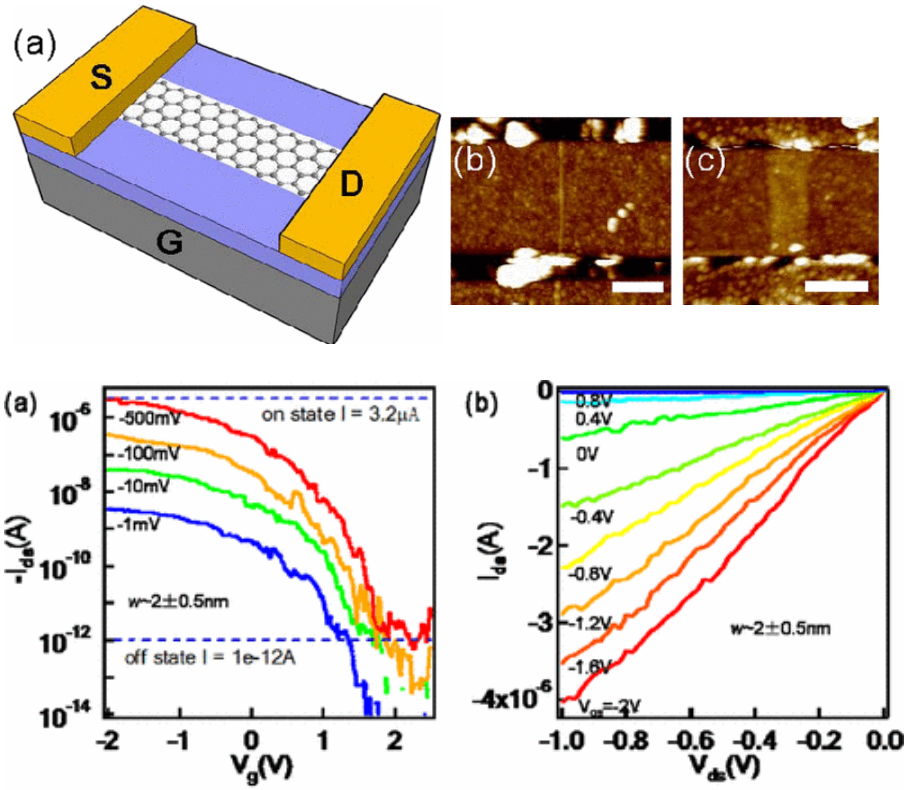

NANO LETTERS Letter pubs.acs.org/NanoLett

Sub-10 nm Carbon Nanotube Transistor

Aaron D. Franklin,*[,†] Mathieu Luisier,[‡] Shu-Jen Han,[†] George Tulevski,[†] Chris M. Breslin,[†] Lynne Gignac,[†] Mark S. Lundstrom,[§] and Wilfried Haensch[†]

[†]IBM T. J. Watson Research Center, Yorktown Heights, New York 10598, United States

[‡]Integrated Systems Laboratory, ETH Zurich, 8092 Zurich, Switzerland

[§]School of Electrical and Computer Engineering, Purdue University, West Lafayette, Indiana 47907, United States

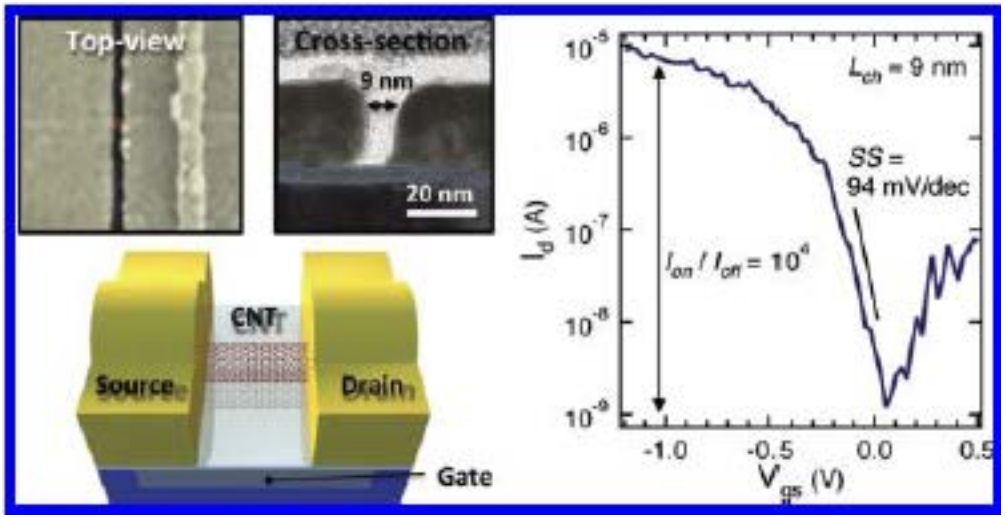

Crossed Nanowires for Negative Differential Resistance-Based Devices

Nano Res (2010) 3: 387–394
DOI 10.1007/s12274-010-1043-z
Research Article

Aligned Graphene Nanoribbons and Crossbars from Unzipped Carbon Nanotubes

Liying Jiao[1], Li Zhang[1], Lei Ding[2], Jie Liu[2], and Hongjie Dai[1] (✉)

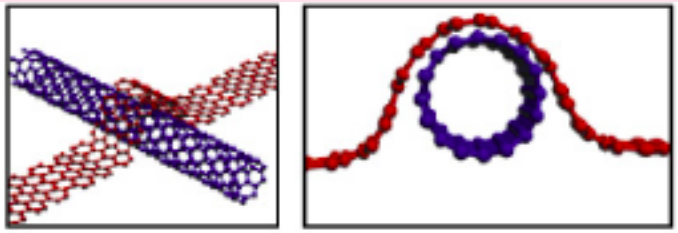

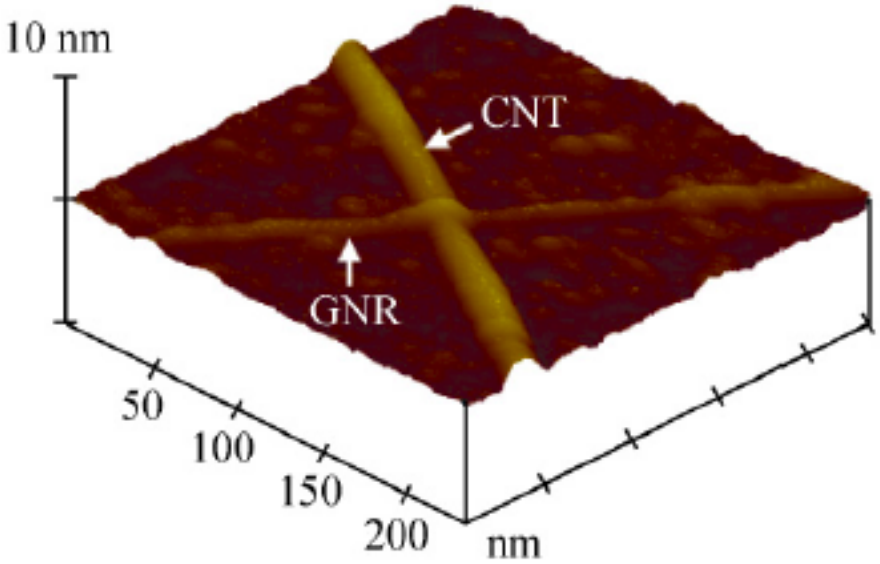

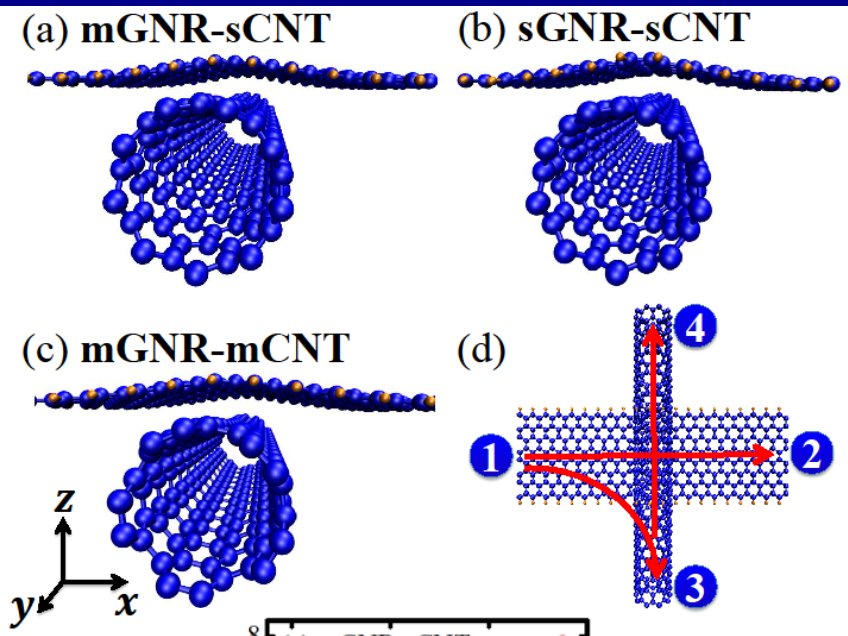

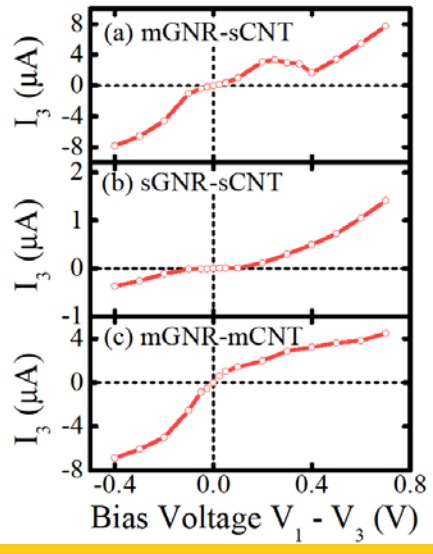

JCEL 12, 542 (2013)

ZGNR Conductance

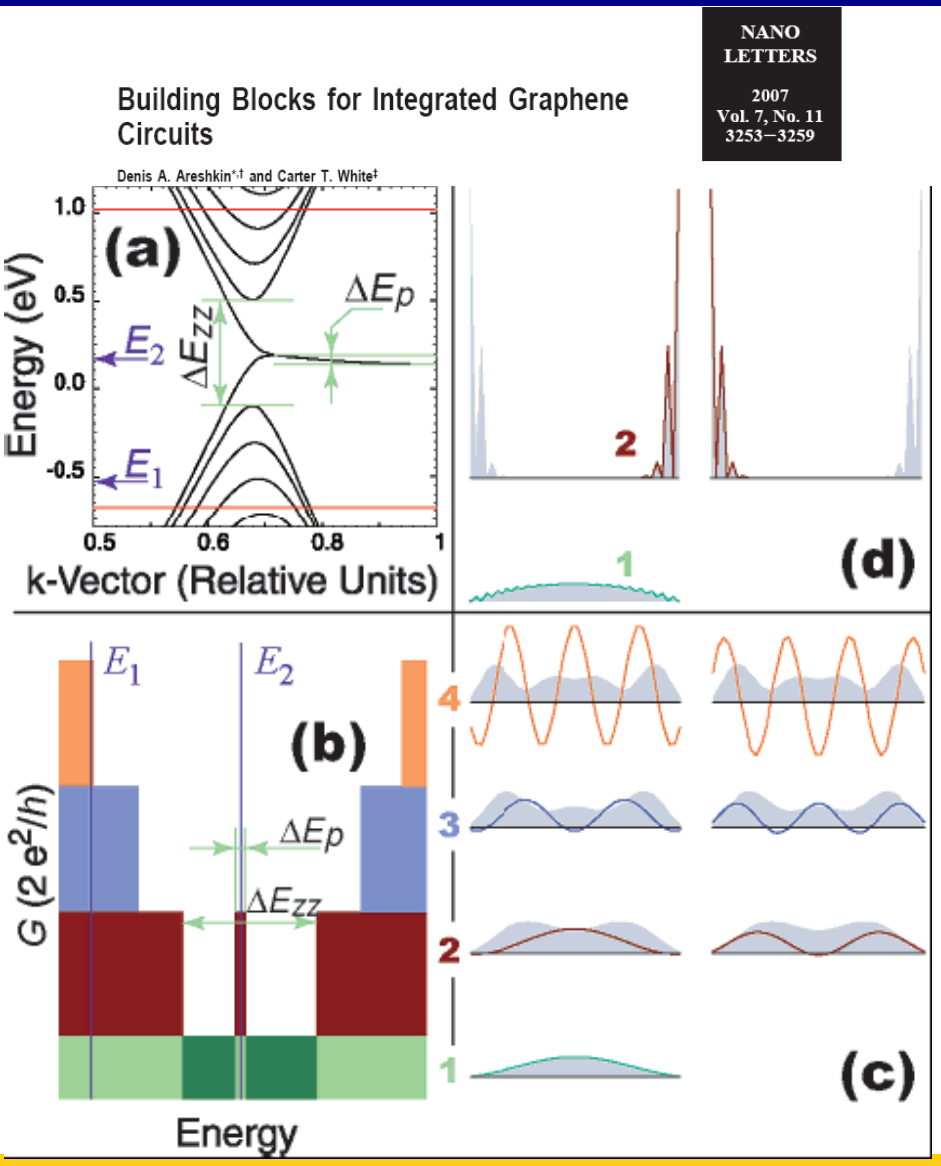

Figure 2. (a) Band-structure for zigzag-edge GNS 40-ZCs wide. (b) Conductance vs energy plot for the energy range marked in pane (a) with red lines. (c) Projected current per unit energy corresponding to energy E_1 vs lateral strip direction for separate conducting channels grouped by the band. All plots are normalized to the same relative scale. Different colors are used to indicate contributions from corresponding bands in pane (b). All bands except the first one give rise to two right moving conducting channels. Shaded regions correspond to the cumulative contribution from the all channels belonging to the same band. Dark-green regions in pane (b) mark single-channel regions. (d) Current per unit energy vs lateral strip direction for separate conducting channels corresponding to energy E_2.

EPL **80**, 47001 (2007)

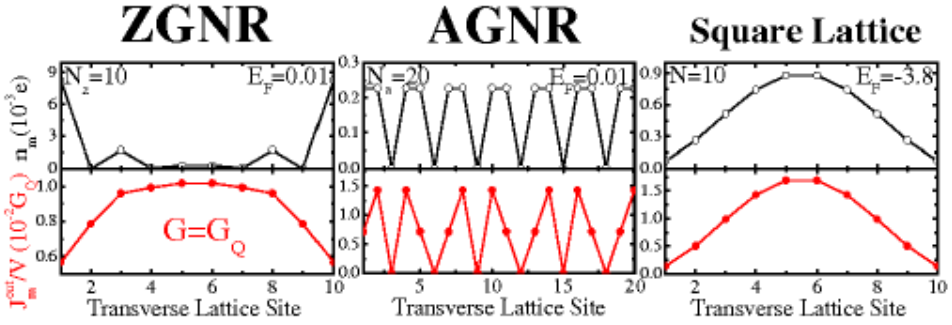

Magnetic Ordering Along Edges of ZGNR via DFT

EPL **80**, 47001 (2007)

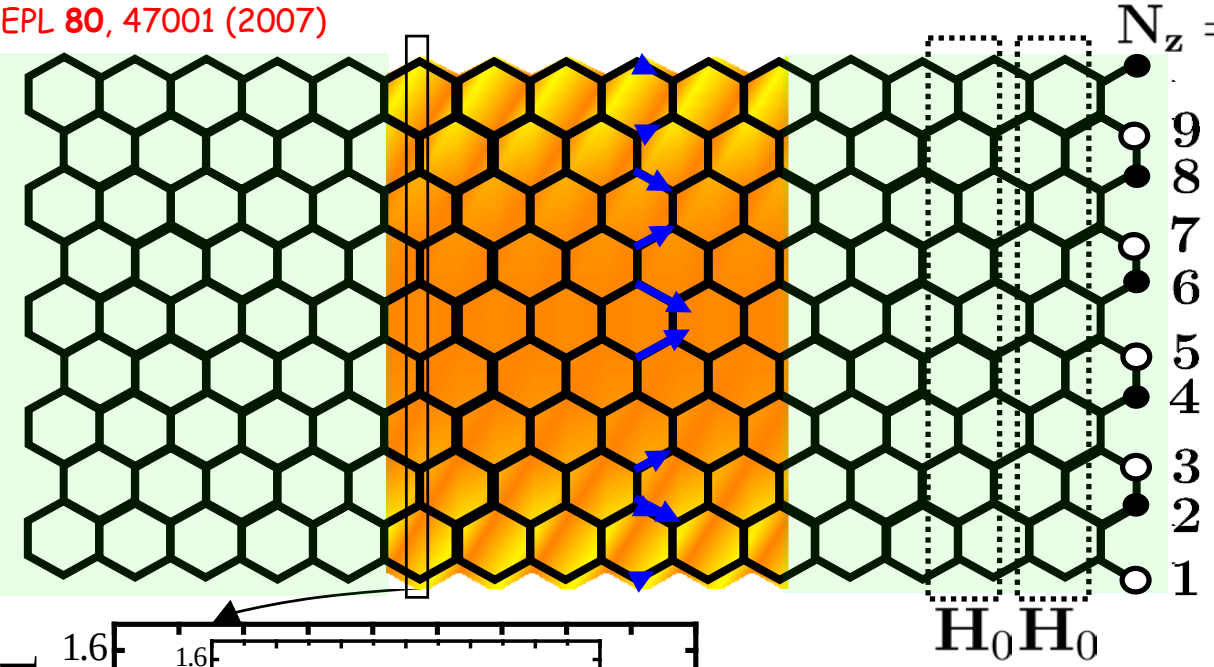

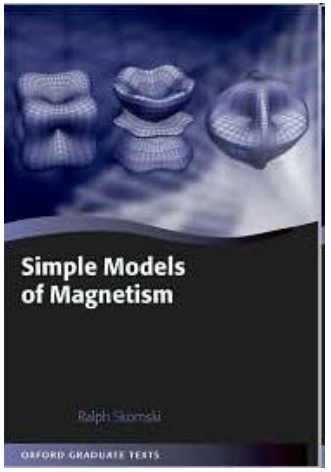

Stoner criterion for itinerant ferromagnetism:

$$U g(E_F) > 1$$

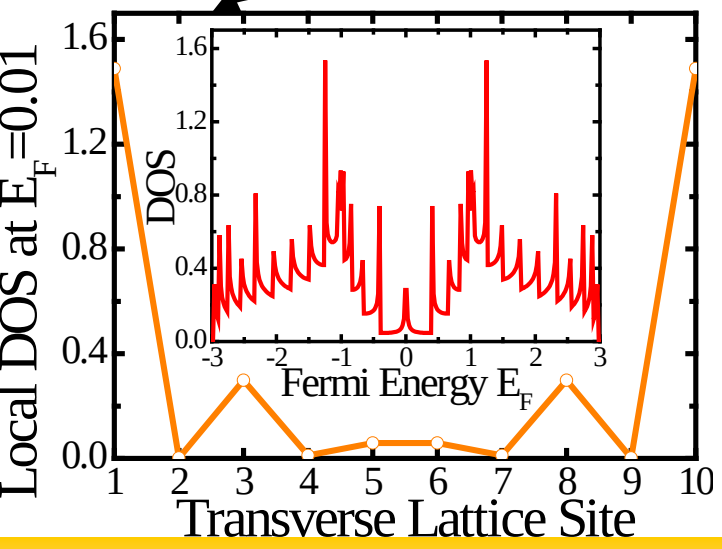

PRL **97**, 216803 (2006)

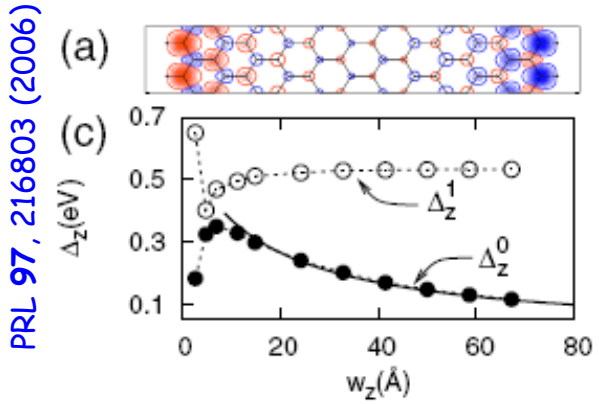

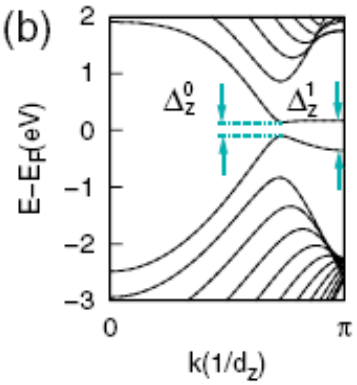

Magnetic Ordering Along Edges of ZGNR Reproduced via Mean-Field Hubbard Hamiltonian

$$\hat{H} = -t \sum_{\langle \mathbf{jl} \rangle} \sum_{\sigma} (\hat{c}^{\dagger}_{\mathbf{j}\sigma} \hat{c}_{\mathbf{l}\sigma} + \hat{c}^{\dagger}_{\mathbf{l}\sigma} \hat{c}_{\mathbf{j}\sigma}) + U \sum_{\mathbf{j}} \hat{n}_{\mathbf{j}\uparrow} \hat{n}_{\mathbf{j}\downarrow}$$

Hubbard model describes electrons hopping on tight-binding lattice + on-site Coulomb interaction between electrons of opposite spin

$$\hat{n}_{\mathbf{j}\uparrow} \hat{n}_{\mathbf{j}\downarrow} \rightarrow \hat{n}_{\mathbf{j}\uparrow} \langle \hat{n}_{\mathbf{j}\downarrow} \rangle + \hat{n}_{\mathbf{j}\downarrow} \langle \hat{n}_{\mathbf{j}\uparrow} \rangle - \langle \hat{n}_{\mathbf{j}\uparrow} \rangle \langle \hat{n}_{\mathbf{j}\downarrow} \rangle$$

Mean-field decoupling of the Hubbard term (equivalent to Hartree-Fock when local spin quantization axis is chosen along the direction of local spin ordering)

PHYSICAL REVIEW B 79, 241401(R) (2009)

Shot noise probing of magnetic ordering in zigzag graphene nanoribbons

Ralitsa L. Dragomirova, Denis A. Areshkin, and Branislav K. Nikolić
Department of Physics and Astronomy, University of Delaware, Newark, Delaware 19716-2570, USA

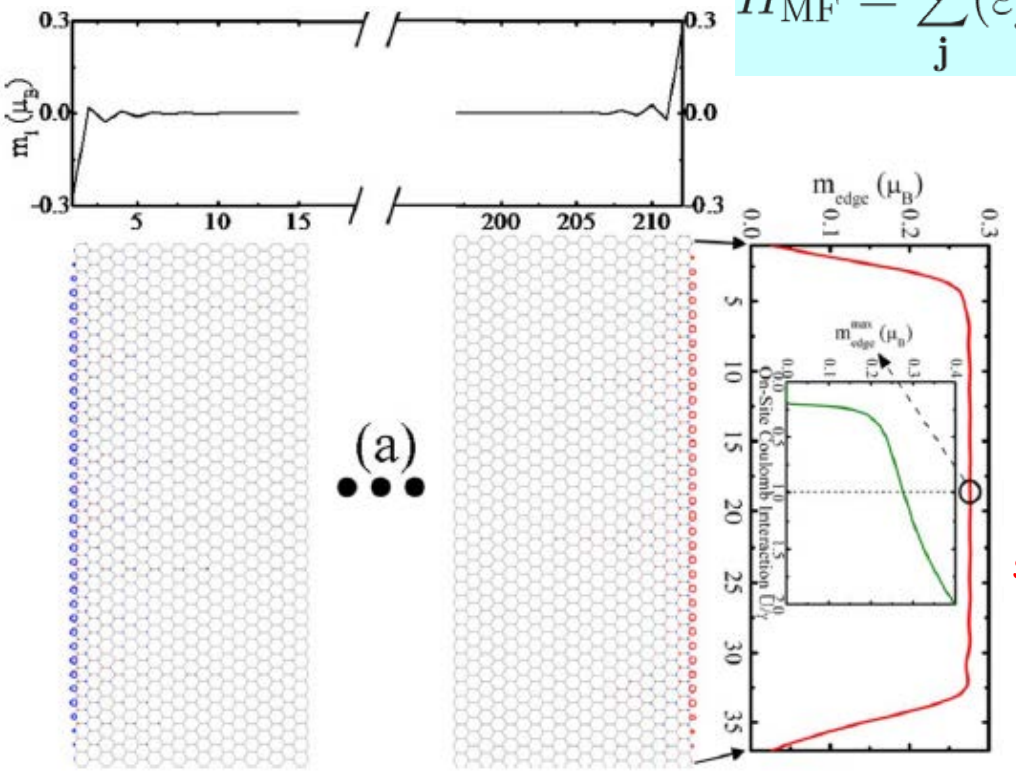

$$\hat{H}_{\mathrm{MF}} = \sum_{\mathbf{j}} (\varepsilon_{\mathbf{j}\uparrow} \hat{n}_{\mathbf{j}\uparrow} + \varepsilon_{\mathbf{j}\downarrow} \hat{n}_{\mathbf{j}\downarrow}) - t \sum_{\langle \mathbf{jl} \rangle} \sum_{\sigma} (\hat{c}^{\dagger}_{\mathbf{j}\sigma} \hat{c}_{\mathbf{l}\sigma} + \hat{c}^{\dagger}_{\mathbf{l}\sigma} \hat{c}_{\mathbf{j}\sigma})$$

$$\begin{pmatrix} \varepsilon_{\mathbf{j}\uparrow} = Un_{\mathbf{j}}/2 - Um_{\mathbf{j}} & 0 \\ 0 & \varepsilon_{\mathbf{j}\downarrow} = Un_{\mathbf{j}}/2 + Um_{\mathbf{j}} \end{pmatrix}$$

$$\begin{aligned} \langle \hat{n}_{\mathbf{j}\uparrow} \rangle &= \frac{n_{\mathbf{j}}}{2} + m, \quad \langle \hat{n}_{\mathbf{j}\uparrow} \rangle = \frac{n_{\mathbf{j}}}{2} - m \\ n_{\mathbf{j}} &= \langle \hat{n}_{\mathbf{j}} \rangle = \langle \hat{n}_{\mathbf{j}\uparrow} \rangle + \langle \hat{n}_{\mathbf{j}\downarrow} \rangle \\ m_{\mathbf{j}} &= \frac{1}{2} (\langle \hat{n}_{\mathbf{j}\uparrow} \rangle - \langle \hat{n}_{\mathbf{j}\downarrow} \rangle). \end{aligned}$$

Self-consistent loop requires spin-resolved particle demsity

$$\begin{aligned} \langle n_{\mathbf{i}\sigma} \rangle &= -\frac{1}{\pi} \int_{-\infty}^{+\infty} dE \, \mathrm{Im} \langle \mathbf{i}\sigma | \hat{G}^{r}(E) | \mathbf{i}\sigma \rangle f(E - E_F), \\ \hat{G}^{r}(E) &= [E - \hat{H}_{\mathrm{MFA}} - \hat{\Sigma}_1 - \hat{\Sigma}_2]^{-1}, \end{aligned}$$

Magnetic Ordering in ZGNR Disappears at Finite Bias Voltage as Nonequilbrium Phase Transition

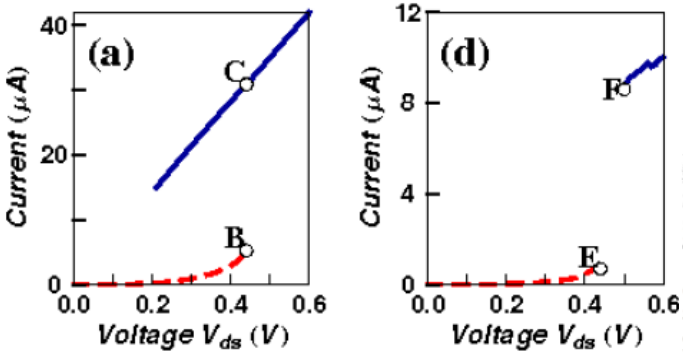

PHYSICAL REVIEW B 79, 205430 (2009)

I-V curve signatures of nonequilibrium-driven band gap collapse in magnetically ordered zigzag graphene nanoribbon two-terminal devices

Denis A. Areshkin and Branislav K. Nikolić
Department of Physics and Astronomy, University of Delaware, Newark, Delaware 19716-2570, USA

Carbon 165 (2020) 476–483

Contents lists available at ScienceDirect

Carbon

journal homepage: www.elsevier.com/locate/carbon

Origin of nonlinear current-voltage curves for suspended zigzag edge graphene nanoribbon

Chunmeng Liu [a], Jiaqi Zhang [a], Manoharan Muruganathan [a], Hiroshi Mizuta [a, c], Yoshifumi Oshima [a], Xiaobin Zhang [b, *]

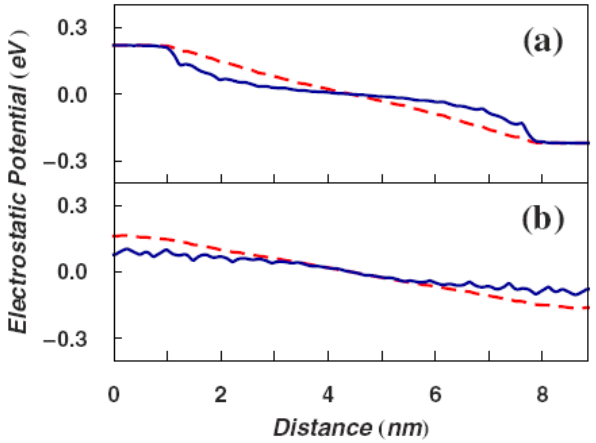

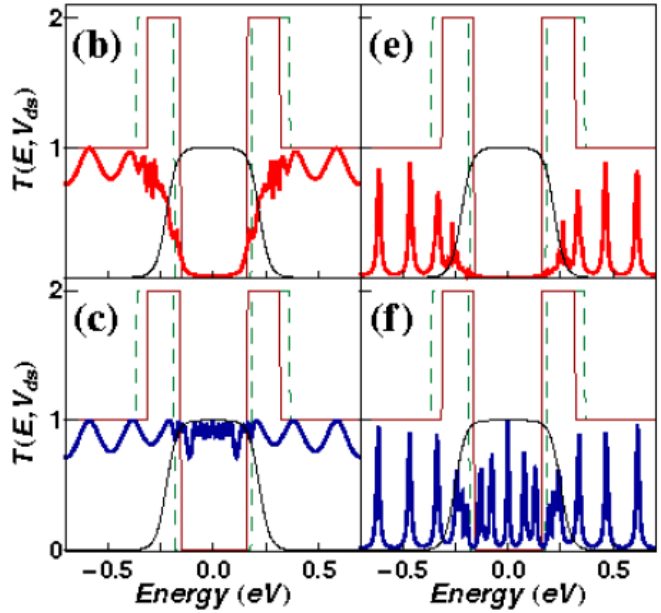

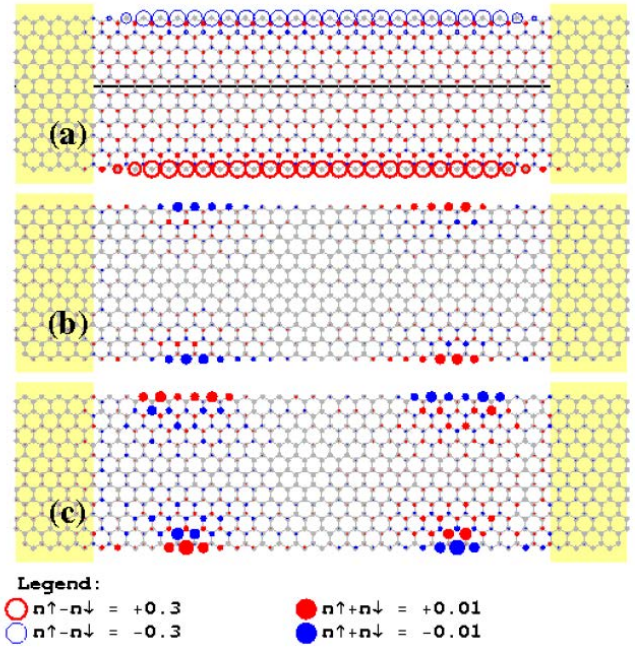

Midgap (E=0) States vs Sublattice Imbalance

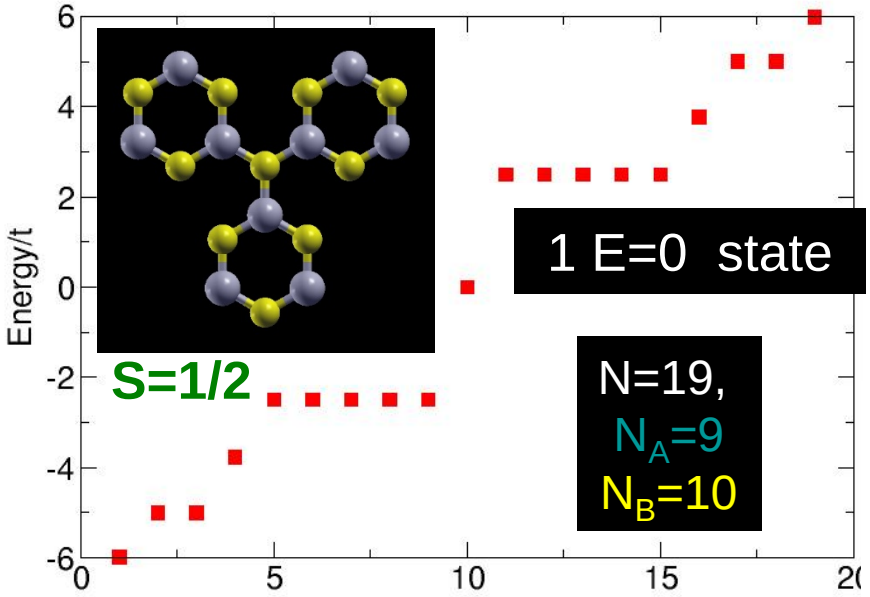

Global sublattice imbalance: $|N_A-N_B|>0$

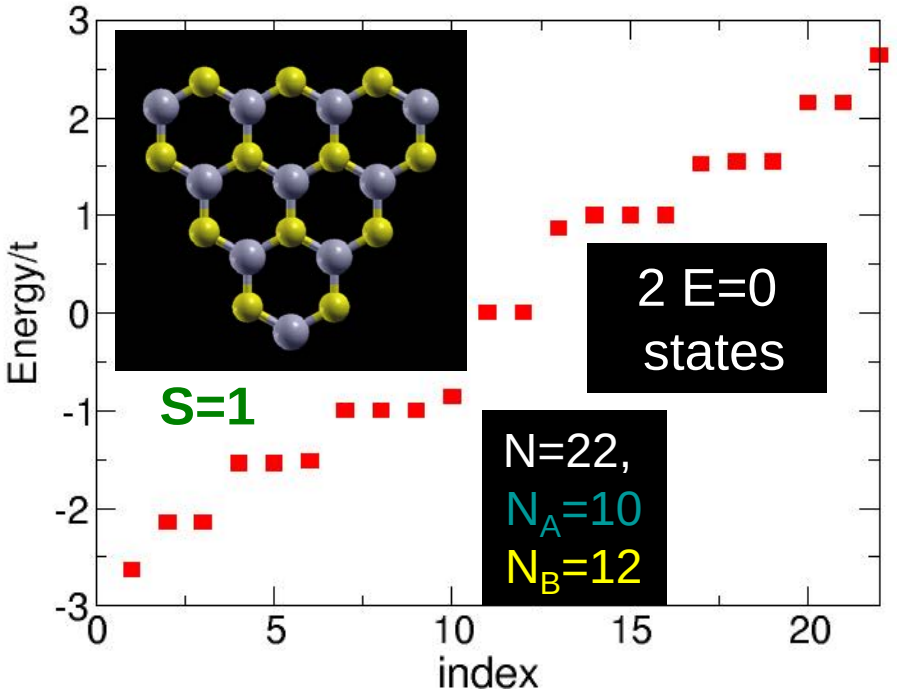

Number of E=0 states in nearest-neighbour TB model on bipartite lattice: $N_z=|N_A-N_B|$

M. Inui, S. A. Trugman, and E. Abrahams, PRB**49**, 3190 (1994).

Zero energy states are sublattice polarized (in majority sublattice).

Courtesy of J. Fernández-Rossier

Electronic Structure in Interacting Picture

- Spin polarization results from Hund's rule and the absence of kinetic energy penalty in sublattice unbalanced graphene structures.

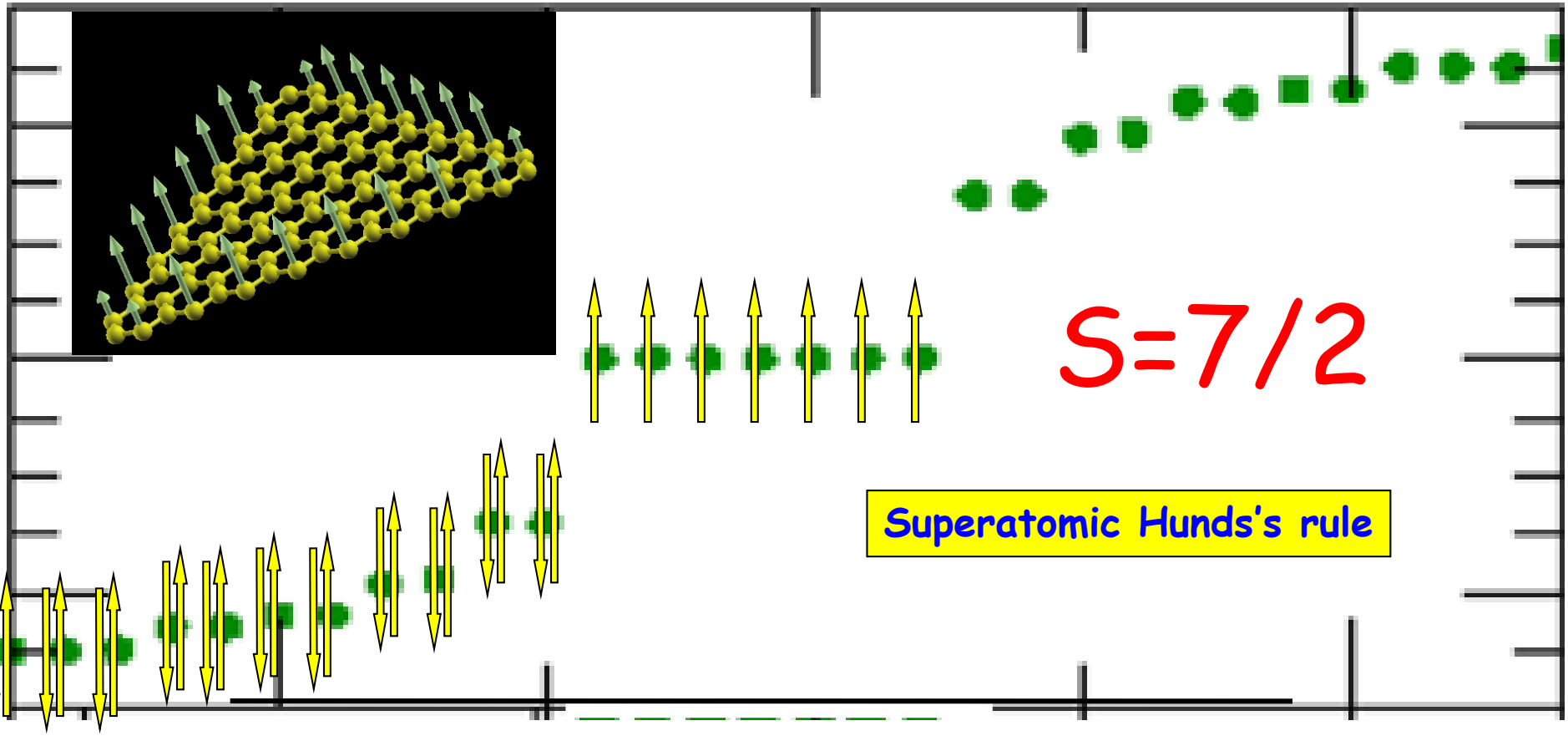

Courtesy of J. Fernández-Rossier

No Sublattice Imbalance S=0 Systems

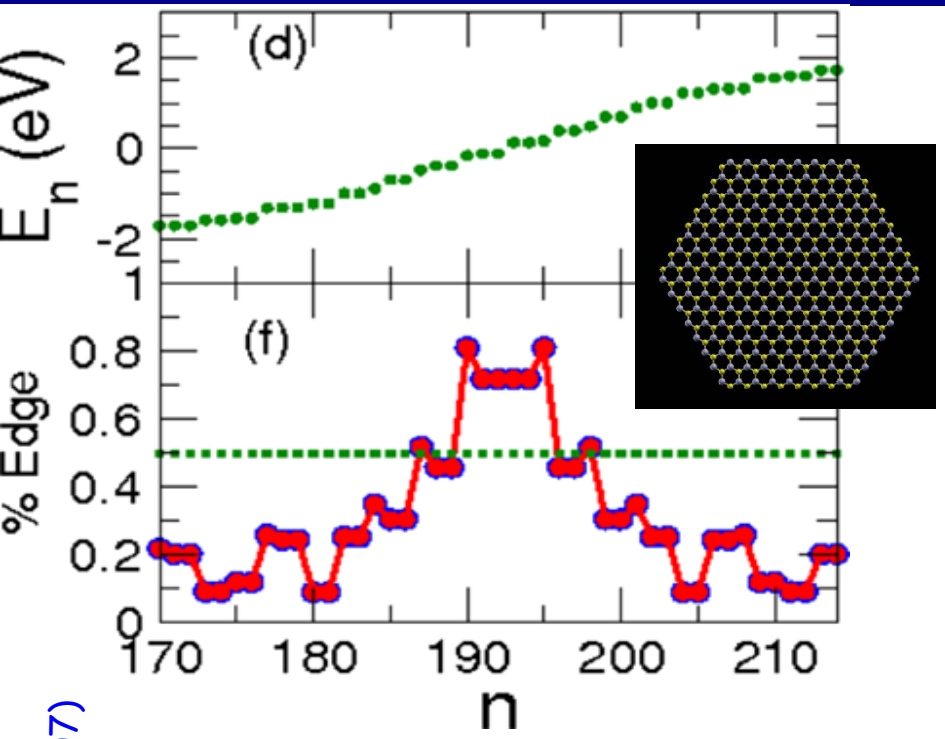

No strict zero energy states

Low energy edge states

0% Sublattice polarized

Low energy states Predominantly on the Edge

Large Hexagons have ferromagnetic edges
Total spin S=0 (AF inter-edge coupling)
Small hexagons have no local moments, larger ones are compensated ferrimagnets (both with S=0)
Competition between Coulomb interaction and AB hybdrization

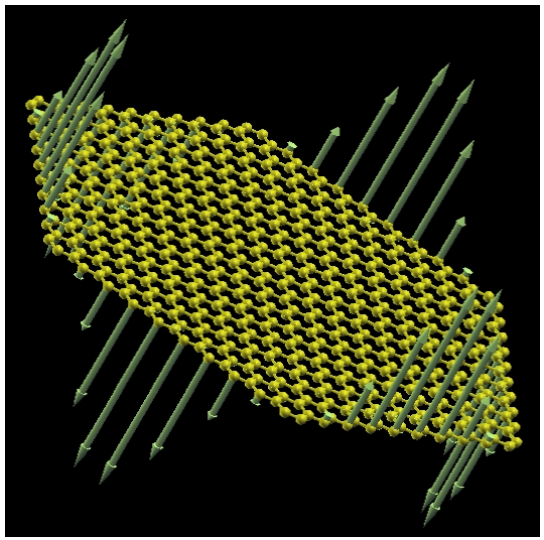

PRL **99**, 177204 (2007)

Courtesy of J. Fernández-Rossier

Crash Course on Spin-Orbit Coupling

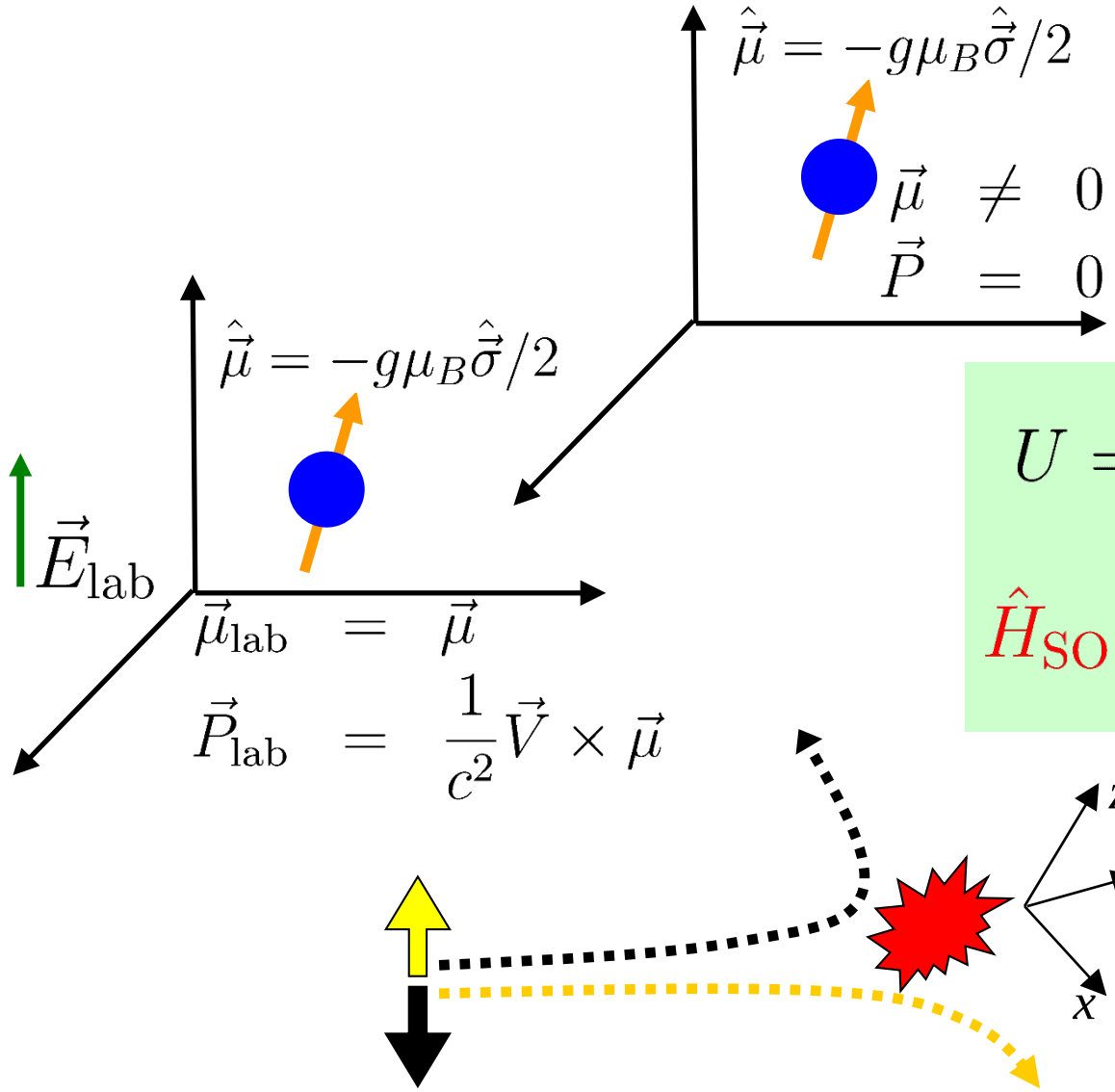

$$U = -\frac{1}{2}\vec{P}_{\rm lab} \cdot \vec{E}$$

$$\hat{H}_{\rm SO} = \frac{e\hbar^2}{4m_0^2c^2}(\hat{\vec{\sigma}} \times \hat{\vec{p}}) \cdot \vec{E}$$

SO deflection force:

$$F_{\rm SO} = \pm P_{\rm lab} \nabla E_x$$

Topological Insulators Predicted Theoretically by Analyzing Band Structure of GNRs with SOC

PRL **95**, 226801 (2005)

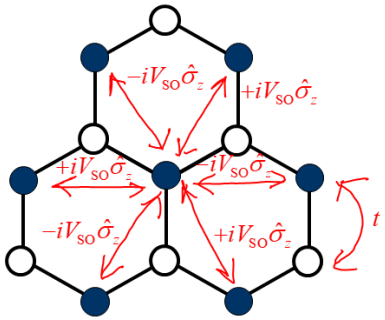

zero SOC

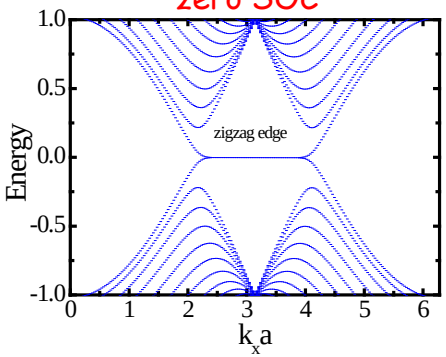

non-zero SOC

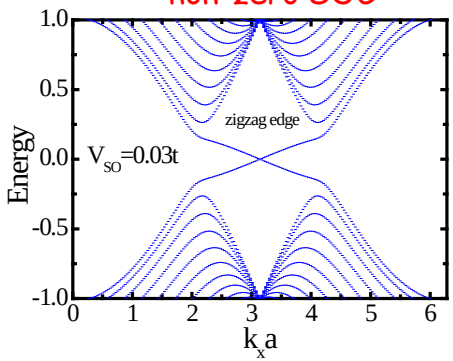

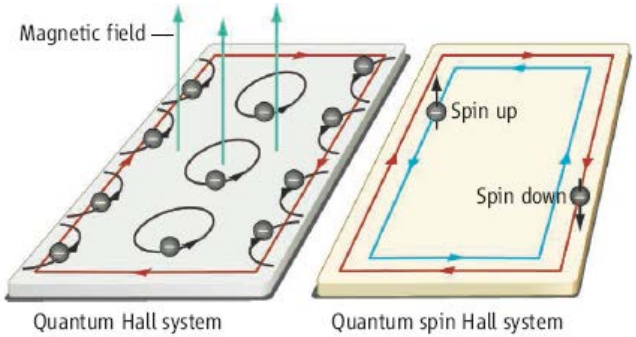

Quantized spin Hall conductance in 4-terminal geometry

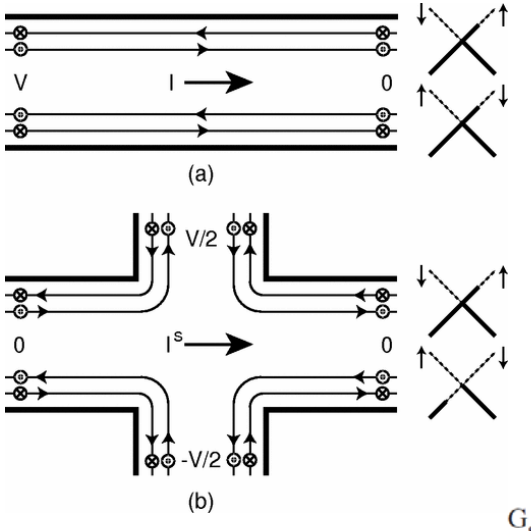

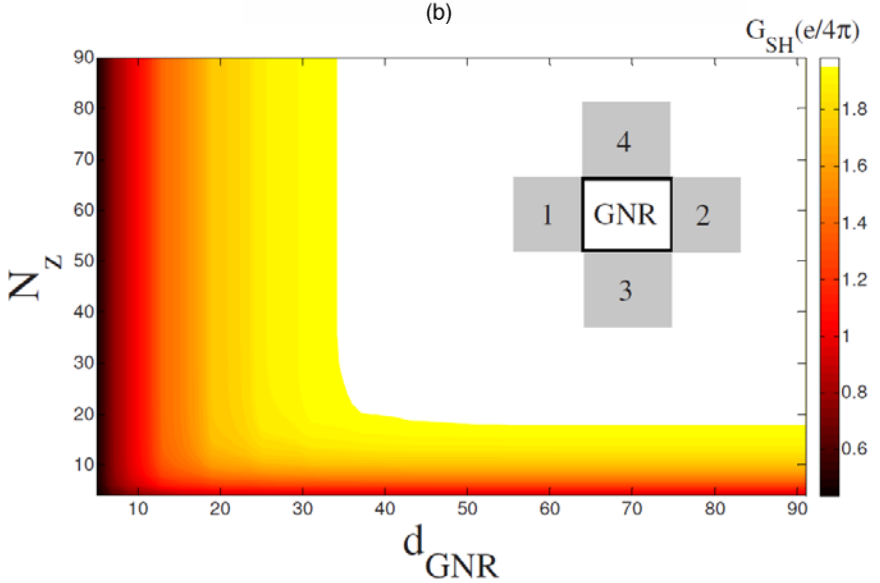

PRB **81**, 035428 (2010)

Where Does Spin-Orbit Coupling in Graphene Comes From: DFT vs. Fitted TB

How big is intrinsic SO coupling in graphene?

Answer: PRB **80**, 235431 (2009) and PRB **82**, 245412 (2010)

Due to a finite overlap between the neighboring p_z and d_{xz} ,d_{yz} orbitals, the intrinsic splitting is linearly proportional to the spin-orbit splitting of the *d* states orbitals higher than *d* have a smaller overlap and contribute less. In contrast, due to the absence of the direct overlap between the p_z and σ-band orbitals, the usually considered spin-orbit splitting induced by the σ-π mixing depends only quadratically on the atomic spin-orbit splitting, giving a negligible contribution

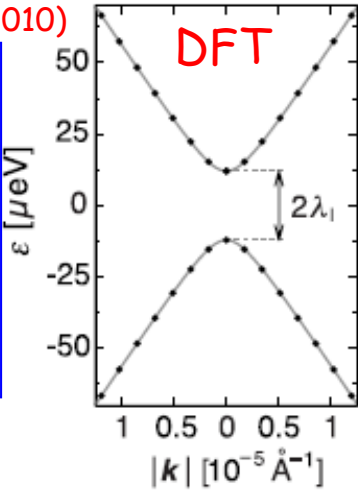

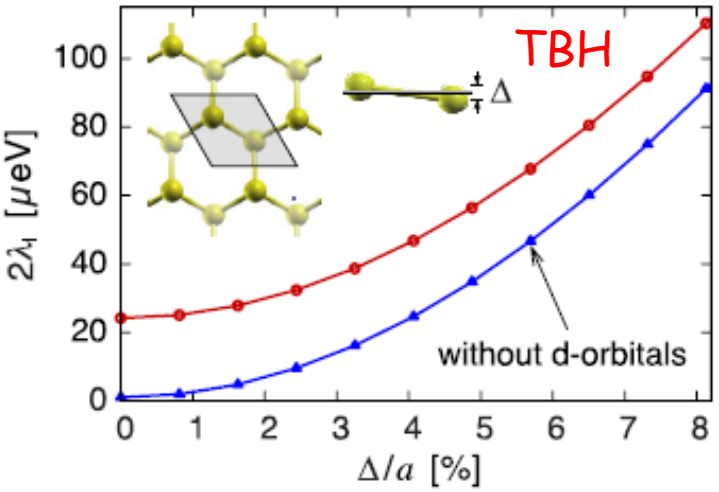

$$H^{SO}_{\ell;\mu,\nu} = \xi_\ell \langle \vec{L} \cdot \vec{S} \rangle_{\mu,\nu}$$

6x6 in the basis p_z, d_{xz}, d_{yz}

$$\begin{bmatrix} H_\pi & H_s \\ H_s^\dagger & H_\sigma \end{bmatrix} =$$

12x12 in the basis $s, p_x, p_y, d_{xy}, d_{x^2-y^2}, d_{z^2}$

$$\begin{array}{cccccc|cccccc}
\varepsilon_p & 0 & 0 & 0 & i\tau\alpha & \alpha & eEz_{sp} & -is_y\xi_p & is_x\xi_p & 0 & 0 & eEz_{pd} \\
0 & \varepsilon_d & 0 & -i\tau\alpha & \beta & i\tau\beta & 0 & 0 & 0 & 0 & 0 & 0 \\
0 & 0 & \varepsilon_d & -\alpha & i\tau\beta & -\beta & 0 & 0 & 0 & is_x\xi_d & -is_y\xi_d & i\sqrt{3}s_y\xi_d \\
0 & i\tau\alpha & -\alpha & \varepsilon_p & 0 & 0 & 0 & 0 & 0 & -is_y\xi_d & -is_x\xi_d & -i\sqrt{3}s_x\xi_d \\
-i\tau\alpha & \beta & -i\tau\beta & 0 & \varepsilon_d & 0 & 0 & 0 & 0 & 0 & 0 & 0 \\
\alpha & -i\tau\beta & -\beta & 0 & 0 & \varepsilon_d & 0 & 0 & 0 & 0 & 0 & 0 \\
eEz_{sp} & 0 & 0 & 0 & 0 & 0 & \varepsilon_s & 0 & 0 & 0 & 0 & 0 \\
is_y\xi_p & 0 & 0 & 0 & 0 & 0 & 0 & \varepsilon_p & -is_z\xi_p & 0 & 0 & 0 \\
-is_x\xi_p & 0 & 0 & 0 & 0 & 0 & 0 & is_z\xi_p & \varepsilon_p & 0 & 0 & 0 \\
0 & 0 & -is_x\xi_d & is_y\xi_d & 0 & 0 & 0 & 0 & 0 & \varepsilon_d & 2is_z\xi_d & 0 \\
0 & 0 & is_y\xi_d & is_x\xi_d & 0 & 0 & 0 & 0 & 0 & -2is_z\xi_d & \varepsilon_d & 0 \\
eEz_{pd} & 0 & -i\sqrt{3}s_y\xi_d & i\sqrt{3}s_x\xi_d & 0 & 0 & 0 & 0 & 0 & 0 & 0 & \varepsilon_d
\end{array}$$

$$\begin{array}{cccccc}
\varepsilon_s & 0 & 0 & 0 & 0 & 0 \\
0 & \varepsilon_p & -is_z\xi_p & 0 & 0 & 0 \\
0 & is_z\xi_p & \varepsilon_p & 0 & 0 & 0 \\
0 & 0 & 0 & \varepsilon_d & 2is_z\xi_d & 0 \\
0 & 0 & 0 & -2is_z\xi_d & \varepsilon_d & 0 \\
0 & 0 & 0 & 0 & 0 & \varepsilon_d
\end{array}$$

GNR + Heavy Adatoms = Realistic 2D Topological Insulator at Room Temperature

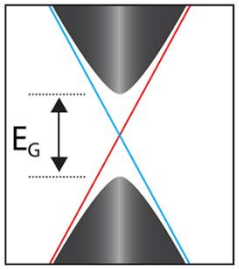

Nano Lett. **14**, 3779 (2014)

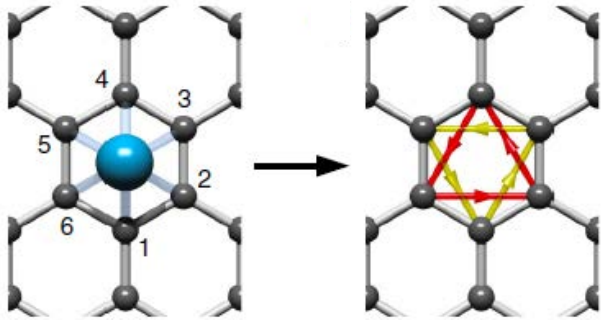

Indium (Z=49) and thallium (Z=81) favor the high-symmetry position and are nonmagnetic, while their partially filled *p* shells ensure that the Rashba SOC they also mediate in graphene is benign at the Dirac points